STRONG, HIGH-TEMPERATURE CERAMICS

CONTRACT N00014-68-C-0323
Office of Naval Research

F. F. Lange

Technical Report Number 11

Metallurgy and Metals Processing Department
Westinghouse Research Laboratories
Pittsburgh, Pennsylvania 15235

February 6, 1974

In press with Ann. Rev. Mat. Sci. 1974

Westinghouse Research Laboratories
PITTSBURGH, PENNSYLVANIA 15235

STRONG, HIGH-TEMPERATURE CERAMICS

CONTRACT N00014-68-C-0323
Office of Naval Research

F. F. Lange

Technical Report Number 11

Metallurgy and Metals Processing Department
Westinghouse Research Laboratories
Pittsburgh, Pennsylvania 15235

ABSTRACT

Strong, high-temperature ceramics are defined as those materials that can withstand thermal cycling without failure which is necessary for their use in high temperature structural applications. For this reason, hot-pressed Si_3N_4 and SiC are emphasized. The relations between fabrication parameters, microstructure and strength are presented for both materials. Other structural considerations, viz., resistance to thermal shock, impact and oxidation are reviewed. Finally, current directions for obtaining improved and new materials are discussed.

INTRODUCTION

The use of ceramic materials for high temperature structural applications is minimal. Early attempts in these areas were unsuccessful. A good example is the post World War II effort to use ceramics in the turbine section of aircraft engines. These early failures must, in part, be attributed to three facts: 1) the lack of suitable ceramics that would withstand the stresses developed during thermal transients; 2) the unavailability of design tools for determining the stresses developed in critical components; and 3) the research and development efforts leading to the emergence of superalloys and cooling technology, which have temporarily solved many of the material problems. Since these early attempts, strong ceramics resistant to moderate and severe thermal shocks have been developed to the stage of commercial[1*]

---

* Superscript numbers denote footnotes.

availability (1).* Design concepts (2,3,4) developed for brittle materials during the interceding period are being combined with new design tools such as numerical stress analysis and fracture mechanics. In recent years, the interest in high performance gas turbines for transportation (5) and power generation (6) is again the impetus for investigating structural ceramics and developing the technology for their use.

Candidate ceramics, the subject of this review, must satisfy two general criteria. First, and most obvious, they must be chemically stable in the high temperature, operating ambience. Second, they must have properties for a reliable mechanical design. These property requirements depend on the specific application, but in general, several thermal properties can be used to define a class of candidate materials most likely to survive the transient thermal stresses that arise whenever the material is cycled between room temperature and high temperature ambience. These conditions, which can be very severe in emergencies,

* Bracketed numbers denote references.

are of particular concern because ceramic materials do not usually possess sufficient ductility to relieve large stresses without cracking.

The stresses that arise during thermal transients depend on the changes in the ambience, the size and shape of the body (which will be neglected) and the properties of the material.[2] The ambient change can be characterized by the temperature change (ΔT) and the rate which heat is transferred from the external body surfaces to the ambience defined by a coefficient, h. The maximum stress arises on the surface; compression for heating and tension for cooling. For the case where $h = \infty$, i.e., the most severe thermal shock, the maximum stress has the form:

$$\sigma_\infty = \frac{\alpha E \Delta T}{1-\mu} , \qquad (1)$$

where α, E and μ are the material's coefficient of thermal expansion, elastic modulus and Poisson's ratio, respectively. For less severe and more realistic shocks $h << \infty$, the maximum stresses are:

$$\sigma = \sigma_\infty \, f(\frac{h}{k}) \ . \qquad (2)$$

The dimensionless function $f(\frac{h}{k}) \leq 1$ and exhibits a maximum (f_{max}) as a function of time. The coefficient k is the material's thermal conductivity. When a fixed value of h is considered, f_{max} decreases with increasing k. Thus, for a given thermal shock condition, the transient thermal stresses can be minimized by choosing a material with small values of α, E and μ and a large value of k. Because moderate values of E and μ are desired for structural rigidity and resistance to fracture (see next section), strong ceramics can be classified with the two thermal properties, α and k. It can be shown that for large bodies subjected to severe shocks (large h), α has a more pronounced effect on the thermal stresses than k. Thus, ceramics with small coefficients of thermal expansion are the most desirable candidates for high temperature structural applications. Without question, strength and thermal conductivity are also important properties.

Based on these considerations, silicon nitride (Si_3N_4) and silicon carbide (SiC) have emerged as leading candidates (5,8-10).

Because both materials can be fabricated by one of several methods, there exists a series of materials with different sets of properties represented by the same chemical formula. For example, Si_3N_4 bodies can be formed by reaction-sintering (11-14), hot-pressing, conventional sintering (15) and chemical vapor deposition (16). Each of these methods and their variations produce bodies with different amounts of porosity, different microstructures and therefore, different properties. Although each method has its advantages, either from an economic viewpoint or from a property standpoint, only the dense, strong forms fabricated by hot-pressing will be reviewed.

The advantages of the hot-pressed forms are related to better structural properties. Relative to their porous forms they are stronger (17), exhibit a higher thermal conductivity (9,11) and a greater resistance to thermal shock (18). With regard to dense material formed by other means, the properties of the hot-pressed forms are still advantageous. Both Si_3N_4 and SiC can be fabricated by chemical vapor deposition (CVD) to form thin walled bodies. Mechanical and thermal properties of CVD Si_3N_4

have not been reported. Although small specimens of CVD SiC can exhibit high strength over a wide temperature range (19), the reliability of larger bodies is unpredictable due to a large dispersion in strength values (20). REFEL SiC, a dense form fabricated by infiltrating and reacting molten Si with SiC + C powder compacts (21), is the only current contender to hot-pressed SiC. Unfortunately, its strength falls precipitately at 1400°C where the excess (8-12 volume %) Si melts (22). The principal disadvantage of the hot-pressed forms is the extensive diamond machining required to form engineering shapes. Methods of hot-pressing complex shapes have been proposed (22), but they have not as yet been reduced to commercial practice.

In reviewing hot-pressed Si_3N_4 and SiC, the known relations between fabrication parameters, microstructures and properties will be emphasized in separate sections. Other structural considerations, viz., resistance to thermal shock, impact and oxidation, will then be reviewed. Finally, current directions for obtaining improved and new materials will then be discussed. Before this is started, the general strength relations for brittle materials will be reviewed to avoid repetition in later sections.

BRITTLE BEHAVIOR

Fracture Mechanics

It is well established that the presence of either cracks or crack precursors (inclusions) cause ceramics to fail at much lower stresses than expected from theoretical calculations. The Griffith-Irwin thermodynamic approach[3] to fracture relates the strength (S) to the crack size (c), the elastic modulus (E) and the energy per unit are required to form the new crack surface (i.e., the fracture energy, γ):

$$S = A \left(\frac{2\gamma E}{c}\right)^{1/2} \tag{3}$$

A is a dimensionless, geometrical factor. This relation is more simply expressed as

$$S = A \frac{K_c}{\sqrt{c}}, \tag{4}$$

where $K_c = \sqrt{2\gamma E}$, the critical stress intensity factor, is directly related to the magnitude of the stresses in the immediate vicinity of the crack front. Techniques exist to directly measure S, E and K_c. Using the above relations, values of γ and c can be calculated.

Both equations show that larger cracks result in lower strengths. Equation (3) shows that greater strengths can be obtained

by maximizing the material properties γ and E while minimizing the crack length, c. These three factors are, in part, related to the material's microstructure. Several of these relations are obvious. First, porosity is unwanted since it decreases E. Second, since the crack sizes responsible for the failure of ceramics are closely related to the size of microstructural features, higher strengths are usually obtained when features such as grain size and the size of second phase inclusions are minimized. As it will become evident, fracture mechanics can be used as a tool to understand the strength behavior of a material and to give a direction for improving strength. In this approach, relations between the microstructure and the three strength controlling parameters γ, E and c are sought. These are then related to strength through Eq. (3).

In many materials, the crack size remains unchanged until the fracture stress. In others, cracks will slowly extend during the period of stressing until they reach a critical size where Eq. (4) is satisfied for the given applied stress. At this point in time, crack extension is

catastrophic. This phenomenon is known as sub-critical crack growth (30,31). The strength of this group of materials depends on the time spent under stress. Currently, stress-rupture experiments result in the most accurate strength-time data required for reliable engineering designs. In these, specimens are maintained at different stresses until they fail. This results in a strength vs time plot.

Two other experiments can also be performed to determine the material's susceptibility to sub-critical crack growth. In one, the rate of crack growth is directly measured as a function of the applied stress (28,32). Specimens containing large, measurable cracks are used for these experiments. The results are expressed as the crack velocity (v) vs the stress intensity factor (K) to facilitate a fracture mechanics analysis for failure time predictions. For many materials the following relation is found:

$$v = BK^n, \tag{5}$$

where B and n are constants. The constant n can be used to define the material's susceptibility to sub-critical crack growth, i.e., as n

decreases, the susceptibility to sub-critical crack growth increases. The second type of experiment involves measuring the material's strength as a function of stressing rate (31,33). High stressing rates will result in greater strengths because the crack has less time to increase in size. Using log-log plots of these data and assuming the relation of Eq. (5), it can be shown that the slopes of the resulting curves are equal to 1/n+1, resulting in a measure of the material's susceptibility to sub-critical crack growth. These data are also useful when the engineering application requires strength data at different relatively fast stressing rates, e.g., transient thermal stresses.

The mechanism responsible for this phenomenon will govern the conditions, e.g., the temperature where a material will exhibit sub-critical crack growth. Glass, for example, is susceptible to sub-critical crack growth due to the attack of atmospheric water vapor (34). In liquid nitrogen ambience, where water-glass reaction kinetics are much slower, glass is less susceptible to sub-critical crack growth and therefore it appears

much stronger (35). Likewise, but for different reasons, Si_3N_4 and SiC exhibit lower strengths at high temperatures where they become susceptible to sub-critical crack growth.

Statistics of Strength[4]

Ceramics exhibit a much greater variability in strength relative to ductile materials. Also, the mean strength of smaller specimens is greater than larger specimens. Both of these facts are due to the large variability of crack sizes present in the smaller specimens used for strength measurements relative to the total range of crack sizes and crack orientations present in a large volume. This presents a problem in defining the engineering strength and in comparing data obtained by different investigators who have used different size specimens and different modes of testing. Since no tools are currently available to determine the distribution of cracks, the problem has been approached through statistics. The approach will be reviewed briefly to give the reader a better background to evaluate strength data presented in the following sections.

Let S be the probability that a unit volume of material will survive to uniform tensile stress σ without failure. If two similar volume elements are combined in either a series or parallel arrangement and then brought to the same stress, their probability of survival (S_2) is the product of the two: $S_2 = S^2$. Likewise, for a number of similar elements with a total volume V, $S_V = S^V$. When this concept[5] is applied to a body with an arbitrary shape and stress distribution, the probability of survival can be defined as

$$S_V = \exp\left[-\int_V f(\sigma)dv\right], \tag{6}$$

where $f(\sigma)$ defines the statistical distribution of strengths, obtained by testing many specimens, as a function of stress. After considerable experience, Weibull (37) concluded that

$$f(\sigma) = \left(\frac{\sigma}{\sigma_o}\right)^m \tag{7}$$

was a suitable (but not universal) empirical distribution function.[6] σ_o is a normalizing stress and m is the Weibull modulus. Both σ_o and m are constants for a material with a given distribution of flaws.

The Weibull modulus is the more interesting parameter since it defines the homogeneity of the material with respect to the distribution of cracks. For the case where $m = \infty$, all specimens, regardless of size, will fracture at the same stress; for $m = 0$, each specimen will have an equal chance of fracturing at any stress. Values for ceramics usually range between 5 and 15, whereas values > 25 are common for metals. Thus, in engineering terms, the strength of a ceramic component must be considered in terms of its probability of survival.

It can be shown that the ratio of the mean strength of one testing mode $(\sigma_m)_1$ using a specimen with a volume V_1 relative to a second testing mode $[(\sigma_m)_2, V_2]$ is given by

$$\frac{(\sigma_m)_2}{(\sigma_m)_1} = \left(\frac{L_1 V_1}{L_2 V_2}\right)^{1/m} . \qquad (8)$$

$L_{1,2}$, the load factors for each mode of tensile stressing, are related to the amount of volume in tension. To illustrate this, let us consider the relation between the expected results for 3-, 4-point flexural stressing and pure tension (3 common testing modes), for the case where $m = 8$ (a value reported for Si_3N_4) (38). The respective loading factors (39)

are $L_{3\text{-pt}} = 0.0065$, $L_{4\text{-pt}} = 0.0225$ and $L_t = 1.0$. For equivalent specimen volumes ($V_{3\text{-pt}} = V_{4\text{-pt}} = V_t$), Eq. (8) predicts that the mean strength measured in 3-point flexural loading will be $\sim$ 15% greater than obtained in 4-point flexural loading and $\sim$ 190% greater than in pure tension. As shown later, similar differences are obtained for Si_3N_4 and SiC.

HOT-PRESSED Si_3N_4

Fabrication

Because of the great interest in reaction-sintered Si_3N_4 and on ways of improving its strength, Deeley, et al., (40) discovered that Si_3N_4 powder could be fully densified under moderate pressures at high temperatures with the aid of small additions of MgO. Other additives have also proved successful (40-42). Fabrication of high strength material depends on the type of Si_3N_4 powder used. Most Si_3N_4 powders, manufactured (43) by reacting Si with N_2 at temperatures > 1100°C and < 1500°C, contain a mixture of α- and β-Si_3N_4. After earlier

misinterpretations suggested that the α and β phases were low and high temperature structural forms. Wild, et al., (44) have reported that the structure of α-Si_3N_4 could be refined by incorporating ∿ 1.5 wt % oxygen, suggesting an approximate formula of $Si_{11.5}N_{15}O_{.5}$. They reported that the β-phase was the pure ("low oxygen potential") Si_3N_4. Other evidence suggests that the α-phase need not contain oxygen (45). Also, Si_3N_4 is known to form solid solution compositions with many oxides, e.g., MgO (46), Al_2O_3 (41,47), Ga_2O_3 (48), etc., which have a structure similar to the β-phase. This and other evidence suggests that the α-phase may be the pure Si_3N_4, whereas the β-phase is stabilized with selected impurities. Regardless of the outcome of this current controversy, Coe (49) recognized that powders containing large amounts of α-Si_3N_4 were necessary to reproducibly obtain high strength, hot-pressed material. This has been confirmed by others (50,51).

Details of the hot-pressing procedure are given elsewhere (52); only a few points will be summarized here. The Si_3N_4 powder and the required MgO additive are milled in an alcohol slurry which mixes the

two powders and reduces their mean particle size. During milling, the powder becomes contaminated with a fine dispersion of the preferred milling media, tungsten carbide. The presence of a small amount of SiO_2, either present in the initial powder (53) due to oxidation or formed during milling by hydrolysis is important for current theories explaining densification (54,55). Densification of the dried, pre-compacted powder is performed in a BN coated graphite die which is heated to a temperature between 1600 and 1750°C for a period < 4 hours under an applied uniaxial pressure of $\leq$ 4000 psi. The BN prevents the reaction of Si_3N_4 and graphite.

Since the densification kinetics of both α- and β-phase powders are similar in all respects (55), the details of the initial densification theory, in which the oxygen content of the α-phase was believed to play an important role (54) do not appear to be correct. More recent experiments (55) have only substantiated the basic premise, viz., a liquid phase forms at high temperatures causing rapid atomic rearrangement and thus densification by a solution-reprecipitation mechanism. Due to the

presence of MgO and SiO_2, the composition of the liquid is believed to be a magnesium silicate containing soluble impurities that are present in the initial powder. Since a crystalline magnesium phase cannot be detected after hot-pressing, (54) it is suspected that the liquid phase solidifies to a glass which remains at the grain boundaries and triple points. Transmission electron microscopy has only confirmed the existence of a glass phase at triple points (56,57) but etching studies (55) and other indirect evidence[7] suggests a similar grain boundary phase. An Auguer analysis of fracture surfaces in which successive surface layers were stripped by ion bombardment indicates the presence of a magnesium-calcium silicate boundary phase (57). This same analysis also shows that a proportion of the smaller cations, e.g., Mg, Al, Fe, etc., have diffused into the Si_3N_4 structure during densification. Based on the known structures of various Si_3N_4-metal oxide solid solutions, (47) the diffusion of MgO into the Si_3N_4 structure can explain the structural change of α to β-Si_3N_4 during densification. As it will become evident, the chemistry of the boundary phase plays an important role in governing the high temperature mechanical properties.

Summarizing some of the general microstructural features, strong dense Si_3N_4 is a polycrystalline material with a β-phase crystalline structure. It has a bimodal grain size distribution with an average size of ∿ 1 μ (55,57). A glassy grain boundary phase is believed to be present. Its grain morphology and the presence of second phase inclusions, which are important strength controlling features, will be discussed in later paragraphs. Other features such as the dispersed W-Fe-Si particles and observed dislocations are reported elsewhere (56,57).

Room Temperature Mechanical Behavior

Coe, et al., (38) reported the mean 3-point room temperature flexural strength of 215 specimens as 910 MN/m^2, with a Weibull modulus of 7.9. Recent data for 3-point, 4-point and tensile measurements are 860, 680 and 410 MN/m^2, respectively, in which a value of m = 9.1 was computed from a much smaller specimen population (58). Good agreement was obtained between these data and the values predicted with a Weibull analysis (see Eq. (8)). Similar flexural strengths have been determined by others for commercial and experimental materials. As

discussed, the strength of hot-pressed Si_3N_4 is also dependent on the direction from which specimens are cut relative to the direction of the applied stress during hot-pressing.

A fracture mechanics approach to investigate the relations between the fabrication parameters, the microstructure and the strength of hot-pressed Si_3N_4 has been reported (50). By fabricating materials with either α- or β-phase powders, then measuring the strength, the elastic modulus and the critical stress intensity factor, it was found that material fabricated with α-Si_3N_4 powder had approximately twice the strength and twice the resistance to crack propagation (K_c) relative to material fabricated in an identical manner with β-Si_3N_4 powder (see Table 1). After close scrutiny of microstructural features, viz., crystal structure, grain size, second phase inclusion and impurity chemistry, it was concluded that the only difference between the two materials was their type of grain morphology. Material prepared with α-Si_3N_4 were textured, containing many elongated fiber-like grains which resulted in an irregular fracture surface. The material prepared with the β-Si_3N_4

powder had an equiaxed grain structure and a much smoother fracture surface. This suggested that the elongated grain structure was responsible for the high fracture energy (or K_c), which in turn (see Eq. (3)) was responsible for the high strength of Si_3N_4 hot-pressed with α-phase powder.

This same investigation showed that K_c depends on the method used to prepare the powders for hot-pressing. The reason for this is not known, but it might be speculated that certain milling procedures (or hot-pressing schedules) optimize the development of the desired grain morphology. K_c for the commercial material was reported as $5.1\ MN(m)^{-3/2}$ (50).

The discovery of the elongated grain structures lead to a hypothesis that the uniaxial stressing during hot-pressing might result in a preferred grain orientation and anisotropic strength. An x-ray diffraction analysis confirmed this hypothesis, indicating that the cylindrical axis (the c-axis of the hexagonal β-Si_3N_4) was preferentially oriented perpendicular to the hot-pressing direction (50). A similar conclusion was also reached with a pole-figure analysis (57). Flexural

strength measurements of bar specimens cut perpendicular and parallel to the hot-pressing direction from a large (3 x 15 x 15 cm) block of commercial material showed that the parallel direction was ∿ 25% weaker than the perpendicular direction (50). This strength difference is maintained throughout the temperature range studied (RT-1400°C). Other properties such as the critical stress intensity factor (50), thermal conductivity (59) and thermal expansion (60) also exhibit different values for these two directions. These directional properties appear to be caused by the preferred grain orientation. It has been suggested that the orientation of other microstructural features, e.g., inclusions and the dispersed tungsten phase, may also contribute to these directional properties (57).

The reason for the formation of the elongated grains is uncertain, but two possibilities exist. First, since α-Si_3N_4 is fiberous after nitriding (11,44) many small, fiber-like particles may be retained in the crushed and milled powders to result in elongated grains which are oriented by the uniaxial pressure during hot-pressing.

Second, the elongated grains may form during densification. Preliminary observation of microstructures during different stages of densification (61) and close examination of different Si_3N_4 powders by electron microscopy (62) gives more credence to the second possibility. Also, Lumby and Coe (63) have shown that the achievement of theoretical density is not sufficient to ensure maximum strength. They suggested that the strength develops after longer hot-pressing periods due to grain growth.

One of the most interesting aspects of Si_3N_4 is its large K_c which means it can support much larger cracks without failure relative to other ceramics. This is demonstrated in Fig. 1 which is a representative micrograph of a fracture surface containing a large BN inclusion (110 μ) at the fracture origin. The flexural strength of this specimen (505 MN/m^2) was only a few percent less than the average strength (530 MN/m^2) of a group of similar specimens without inclusions. This observation is significant for two reasons. First, it indicates that the cracks responsible for the failure of Si_3N_4 are several orders of magnitude larger than the average grain size. A fracture mechanics

study of the Si_3N_4-SiC composite system reached similar conclusions (59). Second, this particular inclusion illustrates the close relation between fabrication and strength, i.e., the BN powder used to coat the die walls was incorporated when the Si_3N_4 powder was poured into the die cavity prior to densification. By avoiding these and other types of large inclusions during fabrication, it has been shown that the mean strength of hot-pressed Si_3N_4 can be significantly increased (64).

High Temperature Behavior

At high temperatures, hot-pressed Si_3N_4 exhibits sub-critical crack growth, plasticity and creep. All evidence suggests that these properties are interrelated and due to the presence of the silicate grain boundary phase which becomes viscous at high temperatures, allowing grain boundary sliding and, hence degrading properties. As it will become evident, impurities that are either present in the initial powder or introduced during fabrication, control the viscosity of the boundary phase and therefore, the high temperature mechanical properties.

Figure 2 illustrates the flexural strength (weak direction) vs temperature for two commercial grades of Si_3N_4 (65). As shown, the strength of the HS-110 material, which contains ∿ 10 times the amount of Ca and Al impurities relative to the HS-130 material, begins to degrade at a much lower temperature. At temperatures where the strength degradation is significant, both materials exhibit plastic deformation prior to fracture. At the same temperature, the impure, HS-110 material exhibits more deformation relative to the HS-130 material. Richerson (66), who was involved in the manufacture of both materials has reported similar data without reference to specific impurities.

Sub-critical crack growth has been reported as the phenomenon responsible for the strength degradation of Si_3N_4 at high temperature (65). Direct evidence for this phenomenon was obtained by observing cracks that grew during stressing. The material's susceptibility to sub-critical crack growth was measured (see previous section) by strength vs stressing rate experiments and by obtaining v vs K data. As illustrated in Fig. 3, strength vs stressing rate experiments performed on HS-130 Si_3N_4

show that it is very susceptible to this phenomenon at temperatures $\geq$ 1200°C. Values of n = 10 to 12 are obtained. Similar behavior was obtained from the v vs K plots reported by Evans and Wiederhorn (67) (shown in Fig. 4). These data illustrate that sub-critical crack growth becomes significant at temperatures > 1250°, resulting in values of n = 10 ± 2. Stress-rupture experiments also show that the strength of Si_3N_4 is strongly dependent on the time spent under stress (20,66). Sub-critical crack growth was also reported as the cause for failure under cyclic-loading at high temperatures (88).

At high temperatures the fracture surface topography is significantly different than observed at lower temperatures (65). As shown in Fig. 6, a rough, crack shaped area is always observed. In impure experimental materials, these areas contain secondary cracks which have under cut portions of the material. Some of these portions protrude from the surface indicating that they were plastically deformed during slow crack growth. Occasionally, small inclusions are observed at the center of these areas illustrating that small pre-existing cracks

slowly grow during stressing until they are the size of the rough-shaped area. At this point the cracked specimen can no longer support the applied load and crack extension is catastrophic.

Since the high temperature strength and fracture surface topography were found to be independent of the testing ambience, the mechanism responsible for sub-critical crack growth must depend on the material's microstructure. It has been proposed (65) that the viscous grain boundary phase allows the highly stressed volume of material in the vicinity of the crack front to plastically deform causing the crack to slowly extend by grain boundary sliding. That is, the crack velocity will depend on the rate of formation and the connection of intergranular voids formed at the crack front. This mechanism is consistent with the effect impurities have on the high temperature strength, viz., material containing impurities that lower the viscosity of the grain boundary phase would be susceptible to sub-critical crack growth at lower temperatures and thus exhibit lower strengths relative to purer material.

Based on this hypothesis, Iskoe and Lange (68) hot-pressed pure β-Si_3N_4 (+ 5 wt % MgO) powder in which controlled amounts of different cation impurities (as oxides) were purposely added prior to hot-pressing. The chosen impurities are commonly found in commercial Si_3N_4 powders. As shown in Fig. 6 only CaO had a significant effect of reducing the strength at 1400°C. The CaO also increased the amount of plastic deformation prior to fracture. The relatively pure base-line material was elastic to fracture. It was hypothesized that the larger Ca cations were unable to fit into the Si_3N_4 structure during densification relative to the other impurity cations. They thus remained in the glassy boundary phase to reduce its viscosity and lower the material's high temperature strength as discussed above.

After nitriding semi-conductor grade Si powder (Ca content < 160 ppm) to obtain a relatively pure α-Si_3N_4 powder, and then hot-pressing with the aid of MgO, Iskoe and Lange obtained an average flexural strength (strong direction) of 335 MN/m^2 at 1400°C representing a 40% improvement over the average flexural strength of HS-130 Si_3N_4 fractured at the same temperature, loading rate, specimen size, etc.

The steady-state creep rate is shown in Fig. 7 as a function of inverse absolute temperature. The HS-110 material is much more susceptible to creep than the purer, HS-130 material. Kossowsky (69) has suggested that grain boundary sliding is responsible for the creep behavior and that the viscosity of the boundary phase, which is controlled by the Ca impurity, is the dominant factor. In summary, all evidence suggests that the high temperature mechanical properties of hot-pressed Si_3N_4 are controlled by the viscous grain boundary phase. The viscosity at a particular temperature being controlled by impurities, and more than likely, the required hot-pressing aid. Grain boundary sliding is the suggested mechanism for sub-critical crack growth, plasticity and creep.

HOT-PRESSED SiC

Fabrication

Formed at temperatures $\lesssim$ 2000°C, SiC has a cubic structure known as β-SiC; when formed at higher temperatures, it exists as a hexagonal structure which has many polytypes all generally classified

as α-SiC (70). As discovered by Alliegro (71), et al., both α- and β-SiC type powders can be densified by hot-pressing with the aid of a second phase additive. The most commonly used additives are Al (elemental or Al_2O_3) and B (72) (elemental, B_4C or H_3BO_4). Manufacturers of hot-pressed SiC prefer the Al_2O_3 additive since B can result in uncontrollable grain growth at a temperature only slightly higher than that required to obtain full densification. Prochazka (73) has recently suggested that the grain growth phenomenon, which results in an undesirable large-grain, low-strength material, might be controlled by a grain growth inhibitor such as carbon.

For the case of the Al_2O_3 aid, SiC powder with an average particle size $\leq$ 3 μm containing $\geq$ 2 volume % Al_2O_3 (incorporated by milling, etc.) can be fully densified at temperatures $\geq$ 1950°C with an applied pressure of 4000 psi (74). Larger particle size powders require high temperatures. A polished and etched section of a material hot-pressed with 10 volume % Al_2O_3 is shown in Fig. 8. The lighter colored phase, which appears to have been a liquid during densification,

wets the darker SiC phase. The curved interfaces suggest that the SiC was taken into solution during densification. These observations strongly suggest that a liquid phase forms at high temperatures causing densification by a solution-reprecipitation mechanism. Upon cooling the second phase remains at the grain boundaries and triple points. The second phase can also be observed as long (< 0.5 cm), narrow (15-30 μ) streaks[8] on polished sections, which form as a result of the liquid being squeezed into irregular, laminar void spaces present in the pre-pressed powder compacts. These streaks have been identified as a Al and O rich second phase by an electron microprobe analysis. This evidence and an x-ray diffraction analysis strongly suggest that this lighter colored phase is Al_2O_3. Indirect evidence also suggests that an alumino-silicate glass is present as a third phase. This is not unreasonable since untreated SiC powder will contain SiO_2 when exposed to air. The average grain size can range between 0.5 to > 20 μ depending on the hot-pressing temperature and the amount of Al_2O_3 incorporated. Dense SiC hot-pressed with Al_2O_3 has an equi-axed grain structure.

For the case of the B aid, the relations between the starting powder, the temperature required for densification and the resulting microstructure are not clearly understood. Several relations are known. First and most consistently observed, large particle size (> 5 μ) SiC powders containing $\geq$ 1 wt % B will not densify at temperatures $\lesssim$ 2100°C (73,74). Material densified at higher temperatures is composed of large (> 30 μm and occasionally $\sim$ 1 mm) plate-like grains which results in a relatively low strength material. Second, sub-micron size β-SiC powders (with surface areas $\geq$ 15 M^2/gm) can be hot-pressed at 1950°C with small additions of either elemental B or H_3BO_3 (75). Prochazka and Charles (75) have observed the following relations. Sub-micron powder that contains a significant amount of oxygen (presumably as SiO_2) result in an equi-axed grain structure with an average grain size of $\sim$ 3 μm. A silicate phase was observed at triple points in this material. Similar powders in which the SiO_2 was removed by leaching, resulted in a microstructure containing many large plate-like grains within a matrix of much smaller grains. Carbon additions were found to suppress the unwanted, exaggerated grain

growth phenomenon. Whatever the cause, the microstructure of SiC hot-pressed with a B aid appears to be very sensitive to impurities and temperature.

Room Temperature Strength

Strong, hot-pressed SiC has only recently become available as a commercial material (1); thus, fewer engineering data exist for this material relative to Si_3N_4. The commercial material, which is densified with the aid of Al_2O_3 (or elemental Al) has all the microstructural features mentioned in the previous paragraphs, viz., an equi-axed grain structure, an average grain size of $\sim$ 2-3 μm (74,78) and a second phase principally observed triple points. Strength measurements determined in 3-, 4-point flexural and tensile modes of stressing have been reported as 760 MN/m^2 (76,1), 660 MN/m^2 (77) and 310 MN/m^2 (78), respectively. Values obtained by flexural loading can exhibit significant scatter due to large cracks which are introduced into the edges of the bar specimens during diamond cutting (77). As illustrated in Table 2, the scatter can be minimized and the average strength increased by

careful grinding and beveling the edges prior to testing. Edge cracks were shown to be a strength-limiting factor for material hot-pressed with the aid of B (75). Strength and other properties of the commercial material are isotropic relative to hot-pressing direction, due presumably to its equi-axed grain structure (77).

The critical stress intensity factor has been reported for a number of different hot-pressed SiC materials (78). For the commercial material, K_c = 4.1 $MN/m^{-3/2}$. Similar values have been reported for other experimental material with a similar grain size (79). Values for materials with a large grain size are much lower (2.6 $MN/m^{-3/2}$) indicating that optimum fracture toughness is obtained for smaller (< 10 μ) grain size material (77). The elastic modulus of hot-pressed SiC is 4.42 x 10^5 MN/m^2 (9). Using this value, the fracture energy (γ) of commercial SiC is 19.5 N/m which is typical of other equi-axed, polycrystalline ceramics.

Large second phase inclusions are rarely observed at fracture origins in the commercial material primarily because fracture origins

are located at the edge of bar specimens due to cracks introduced during machining. Irregular shaped pockets of the Al_2O_3 second phase have been identified at fracture origins (77). When the Al_2O_3 is well dispersed and confined to sizes less than several microns, it has been shown not to effect the strength regardless of its volume content within the material (see Fig. 9). Attempts have been made to correlate the crack size responsible for failure with the largest grain observed within the fracture origin. These correlations are in reasonable agreement with values predicted from a fracture mechanics calculation when large SiC grains are either purposely (77) or accidently (by exaggerated grain growth) incorporated (79) into a fine grain matrix. Also, materials with a large average grain size are weaker (77,79).

In summary, the room temperature strength of hot-pressed SiC is strongly dependent on the size of microstructural features, e.g., grain size, which can easily be altered by changing the fabrication parameters. High strengths can be obtained from materials with a uniform grain size of $\sim$ 3 μ. Extreme care must be taken to avoid introducing large edge cracks while machining test specimens.

High Temperature Behavior

The strength of commercial material decreases with increasing temperatures as shown in Fig. 10 (77). At temperatures $\geq$ 1200°C, sub-critical crack growth is, in part, responsible for the steady decline in strength (77). Evidence for this phenomenon, obtained from strength vs stressing rate experiments, is shown in Fig. 10. The material's susceptibility to sub-critical crack growth measured by this technique is n = 21 ± 3 between 1200 and 1400°C. Since data has not been reported at lower temperatures, the temperature where this phenomenon first appears is uncertain. The decrease in K_c from 4 $MNm^{-3/2}$ at 1000°C to 3 $MNm^{-3/2}$ at 1400°C is also responsible for strength degradation within this temperature range (77).

Because identical strengths are obtained in air, argon and vacuum at 1400°C (77) the mechanism responsible for the sub-critical crack growth appears to be related to the material's microstructure. As shown in Fig. 9, the amount of the Al_2O_3 hot-pressing aid does not greatly influence the high temperature strength. Although these data

do not preclude the possible effects of Al_2O_3 on slow crack growth, the introduction of CaO to SiC (plus 2 volume % Al_2O_3) powder prior to hot-pressing was found to have a significant effect (77). Strength vs stressing rate data shown in Fig. 10 illustrate that this impurity increased the material's susceptibility to sub-critical crack growth from a value of n = 21 (commercial material with < 100 ppm Ca) to n = 6. The CaO addition also caused the specimens to plastically deform prior to fracture and resulted in rough crack-shaped areas on the fracture surfaces similar to that found for Si_3N_4 (see Fig. 5).

Flexural strength data have been reported by Prochazka and Charles (79) for two experimental materials fabricated with the aid of B. One of these was observed to contain a silicate grain boundary phase. Although the low temperature strengths of these materials were less than the commercial material, neither were affected by temperature until about 1400°C. At higher temperatures the material containing the silicate phase was the first to degrade.

It is important to note that SiC is not intrinsically weak at high temperatures. The strength of CVD SiC is unaffected by temperature up to 1600°C (19). Since this type of material is relatively purer than hot-pressed materials, it is not unconceivable to suggest that impurities and hot-pressing aids are responsible for strength degradation. Sub-critical crack growth occurs in the hot-pressed material at high temperatures. It has been shown that impurities, e.g., CaO, effects this phenomenon. These observations strongly suggest that a viscous grain boundary phase is responsible for slow crack growth, which in turn results in lower strengths at high temperatures.

OTHER STRUCTURAL CONSIDERATIONS

Thermal Shock Resistance

As discussed in the introduction, the stresses that arise within a body during a thermal transient condition are related to the properties of the material, the size and shape of the body, and the change in the ambience. Due to the complexity of these relations,

several simplified parameters are used in ranking materials with respect to their resistance to thermal shock (7). Knowledge of certain material properties, viz., strength, elastic modulus, Poisson's ratio, thermal expansion and thermal conductivity, are required in calculating these parameters. Si_3N_4 and SiC are highly ranked by such ratings (8). Simple thermal shock experiments (relative to actual operating conditions) are also used in ranking materials. Many of these involving Si_3N_4 and SiC have gone unreported because of their cursory nature. Among those that have been reported, the gas burner experiments of Sanders and Probst (10) appear to be the most pertinent as related to the projected applications of these materials. Cylindrical specimens of 23 oxidation resistant ceramics were systematically immersed into a hot (1200°C), high-velocity (Mach 1), gas stream. Dense Si_3N_4 and SiC survived isothermal and cyclic tests without any signs of cracking. Other materials failed due to thermal or mechanical (gas loading) stresses. In a different approach, Schaller and Rahaim (80), have computed the transient thermal stresses that arise within a turbine vane subjected

to rapid cooling. Known ambient changes, material properties and size-shape considerations were related through computer modeling. The stresses were calculated using two dimensional finite element and finite difference methods. The material properties used were those reported for hot-pressed Si_3N_4 and SiC. Their results showed that despite their different properties (Si_3N_4 has lower values of thermal expansion and elastic modulus, whereas SiC has a higher thermal conductivity) similar stresses (within 10%) arise in both materials for an average heat transfer coefficient (h) of 0.06 cal $sec^{-1}{}^{\circ}C^{-1}cm^{-2}$. The maximum stress depended on the initial temperature. If the statistical strength behavior of a material is known, this type of an analysis can be used to estimate the components chances of surviving a particular thermal shock. Such an analysis is also required in designing proof testing procedures to ensure the reliability of a component for given period of operation (81).

Impact Resistance

The forces exerted by an impacting object can induce two types of damage. First, stress waves arise within the entire body that may cause failure. Second, if failure does not occur, surface cracks can be introduced by the highly localized stresses at the position of contact. These cracks lower the strength of the body when it is subsequently loaded to failure. A third phenomenon can also occur, viz., the impacting body can shatter without inflicting damage.

Ballistic impact experiments were performed on Si_3N_4 by this author. Rectangular plates (1.27 x 5.08 cm) with thicknesses of either 0.635 cm or 0.317 cm were simply supported at each end (support span = 3.81 cm) and impacted with steel spheres (either 0.159 cm or 0.317 cm in diameter) traveling at 100 ± 10 M/sec. Only the thicker plates impacted with the smaller spheres survived. The surviving plates contained visible Hertzian ring cracks which resulted in a strength reduction of $\sim$ 25% after a subsequent flexural strength measurement. Graphite spheres (0.317 cm dia.) shattered upon impact without inflicting damage.

The relative resistance of commercial Si_3N_4 (weak direction) and SiC to surface damage inflicted by Hertzian contact stresses has been determined by using 0.317 cm diameter steel spheres as indenters (82). The critical force required to induce surface damage was detected by subsequent strength measurements. The results shown in Fig. 11 illustrate that 4 times the force was required to inflict damage into Si_3N_4 relative to SiC. Once surface damage was introduced, SiC exhibited a greater rate of strength degradation for larger indentor forces. It should be noted that both materials had a similar strength prior to the introduction of surface damage. Although the criterion for the formation of Hertzian cracks is not well established, several theories suggest that the critical force depends on the material's fracture energy (83,84). Thus, because of its greater fracture toughness, Si_3N_4 is significantly more resistant to impact damage relative to SiC. High-velocity sand erosion studies (85) have also ranked hot-pressed Si_3N_4 above other materials including plastics, metals and other ceramics. Experiments are currently underway to access the durability of Si_3N_4 for bearing applications (86).

High Temperature Stability

Although neither material is thermodynamically stable in oxygen environments, both form stable silicate surface layers to render them resistant to oxidation for extended periods. Examples of the oxidation behavior for commercial Si_3N_4 and SiC at 1260°C and 1370°C as reported by Singhal (87) are shown in Fig. 12. Both exhibit a parabolic rate law, indicating that the reaction is limited by a diffusional process through a surface layer. The oxidation resistance of both materials are similar over the temperature range shown. Their resistance to high temperature, high velocity gas turbine environments has also been demonstrated (87). The hot-pressing aid and impurities have a major role in determining the composition of the protective silicate surface layer. For the case of Si_3N_4, Mg and Ca cations diffuse to the surface to form glassy and crystalline phases (88,89). For SiC hot-pressed with Al_2O_3, an alumino-silicate glass, modified with potassium has been identified (90). The glass phases, which are viscous at high temperatures govern the rate of oxidation. Thus, impurities and hot-pressing aids that react with

SiO_2 to form viscous silicates will have a profound effect. For example, Singhal has shown that the oxidation rate of HS-110 Si_3N_4 is $\sim$ 3 times greater than the purer HS-130 material. The amount of the Al_2O_3 hot-pressing aid also has an important effect on the oxidation rate of SiC (90).

Very little has been reported concerning the stability of either material in reducing, inert and vacuum ambients. At temperatures > 1500°C, Batha and Whitney (91) have reported that Si_3N_4 powder dissociated in vacuum and nitrogen ambients. SiC is known to preferentially sublime Si in vacuum (92).

CONCLUDING REMARKS

Currently, the principal differences between hot-pressed Si_3N_4 and SiC can be viewed as follows. Hot-pressed Si_3N_4 has a greater fracture toughness than SiC. This is the apparent reason why Si_3N_4 is less susceptible to surface damage inflicted during machining and ballistic impact. Based on their differences in K_c, Si_3N_4 can support a larger crack (or crack precursor) without failure. Although second

phase inclusions are unwanted in either material, less care need be taken in avoiding moderate size (∿ 100 μ) inclusions in Si_3N_4. When care is taken, the mean strength can be raised to higher levels (64).

On the other hand, Si_3N_4 is more susceptible to sub-critical crack growth and based on preliminary data for SiC (73,93) less resistant to creep at high temperatures. Several approaches are being taken to improve the high temperature mechanical behavior of Si_3N_4. Most of these involve either modifying or eliminating the glassy grain boundary phase. In the first approach, attempts are being made to reduce (or eliminate) impurities that lower the viscosity of the glass (68). Calcium compounds have been the prime target since they are one of the major impurities in commercial Si powder (and thus in Si_3N_4 powders) and experimental evidence shows that they have a significant effect in degrading high temperature properties. The success of this approach can be measured by the improved properties of the commercial HS-130 Si_3N_4 over those of the impure HS-110 material and the further improvements reported by Iskoe and Lange (68) for purer material. In the second

approach, different hot-pressing aids are being sought that form more refractory glasses. Gazza (42) has reported that Y_2O_3 is effective in both promoting densification and increasing the high temperature strength relative to similar Si_3N_4 powders hot-pressed with additions of MgO.

The third approach is most interesting since it leads to a new series of low expanding materials based on the known solubility of many oxides in Si_3N_4 (47). For example, the solubility limit of Al_2O_3 in Si_3N_4 was estimated as $\sim$ 70 mole % at 1750°C (46). These materials have an expanded β-Si_3N_4 type of crystal structure believed to be built up of $(Si,M)(N,O)_4$ tetrahedral units (47) that share corners, where M represents the metal cation. Thus, it is conceivable that the unwanted impurities can be incorporated into these expanded structures along with the excess SiO_2 that might otherwise be present in the unwanted grain boundary phase. Preliminary data obtained by this author indicates that certain Si_3N_4-Al_2O_3 solid solutions do not exhibit plastic deformation prior to fracture at 1400°C. Flexural strengths in the range of

45,000 psi are also obtained at this temperature. Impure α-Si_3N_4 powder was used to fabricate these materials. Further effort in this area is required before any firm conclusion can be drawn.

Improved properties have also been obtained by combining the advantages of the low thermal expansion and high fracture toughness of Si_3N_4 with the high thermal conductivity of SiC by forming hot-pressed Si_3N_4-SiC particulate composites (59). When the average particle size of the SiC dispersed phase is < 5 μ, the room temperature strength is relatively unchanged compared to Si_3N_4 without the dispersed phase. At high temperatures the composites were stronger than the matrix material. The thermal conductivity of composites containing 0.30 volume fraction of the dispersed SiC phase was $\sim$ 40% greater than the matrix, suggesting that the Si_3N_4-SiC composite system might have improved thermal shock resistance. Fiber composite approaches are also being studied to increase the impact strengths of Si_3N_4 and SiC. Graphite, metal and ceramic fiber have been incorporated into Si_3N_4 and SiC powders prior to hot-pressing (51,94). Improvements have been reported for some of these

systems, but their long term oxidation resistance appears to be questionable.

The science and technology of strong, high temperature ceramics is a field of great interest and rapid advancement. The mechanisms presented to explain the strength behavior of these materials can be considered new and controversial. On the other hand, they are consistent with current facts and have pointed a direction for material improvements.

LITERATURE CITED

1. Alliegro, R. A., Torti, M. L. 1973. Gas Turbine Int. Jan-Feb:30-36.

2. Dukes, W. H., Anthony, F. M. 1969. Fracture, IV, ed. H. Liebowitz, 275-355. New York:Academic.

3. Barnett, R. L., McGuire, R. L. 1966. Bul. Am. Ceram. Soc. 45:595-602.

4. Stanley, P., Fessler, H., Sivill, A. D. 1973. Proc. Brit. Ceram. Soc. 22:453-487.

5. McLean, A. F. 1973. Bul. Am. Ceram. Soc. 52:464-466.

6. DeCorso, S. M., Harrison, D. E. 1972. Ceramics in Industrial Gas Turbines. ASME Pub. 72-GT-94. Presented at Gas Turbine and Fluids Eng. Conf., San Francisco, California.

7. Sym. on Thermal Fracture 1955. J. Am. Ceram. Soc. 38:1-54.

8. Godfrey, D. J. 1968. Metals and Materials 2:305-311.

9. Lange, F. F. 1972. Dense Si_3N_4 and SiC: Some Critical Properties for Gas Turbine Applications, ASME Pub. 72-GT-56 (see Ref. 6).

10. Sanders, W. A., Probst, H. B. 1972. NASA Tech. Note, NASA TN D-6890.

11. Parr, N. L., May, E. R. W. 1967. Proc. Brit. Ceram. Soc. No. 7, 81-98.

12. Davidge, R. W., Gilling, D., Wilyman, P. R. 1972. Special Ceramics V, ed. P. Popper, 329-344. Stoke-on-Trent, England: The British Ceramic Research Association.

13. Barnby, J. T. see Ref. 12, 311-328.

14. Caws, R. B., Graham, R. P., Stoddart, D. E. 1973. Silicon Nitride Materials for Gas Turbine Components. ASME Pub. 73-GT-47. Presented at Gas Turbine Conf.,Washington, D. C.

15. Terwilliger, G. R., Lange, F. F. 1973. Task II: Pressureless Sintering of Si_3N_4, Final Rept. Naval Air Systems Command, Contract No. N00019-72-C-0278.

16. Galasso, F., Kuntz, V., Croft, J. 1972. J. Am. Ceram. Soc. 55:431.

17. Lloyd, D. E. 1968. Special Ceramics 4, ed. P. Popper, 165-172. Stoke-on-Trent, England: The British Ceramic Research Association.

18. Glenny, E. and Taylor, T. A. 1961. Powder Met. 8:164-195.

19. Gulden, T. D. 1969. J. Am. Ceram. Soc. 52:585-590.

20. McLean, A. F., Fisher, E. A., Bratton, R. J. 1972. "Brittle Materials Design, High Temperature Gas Turbine", Contract No. DAAG 46-71-C-0162, Army Materials and Mechanics Research Center, Interim Report CTR 72-19.

21. Forrest, C. W., Kennedy, P., Shennan, J. V., see Ref. 12, 99-124.

22. McLaren, J. R., Tappin, G, Davidge, R. W. 1972. Proc. Brit. Ceram. Soc. 20"259-274.

23. Lange, F. F., Terwilliger, G. R. 1973. Bul. Am. Ceram. Soc. 52:563-565.

24. McLean, A. F., Fisher, E. A., Harrison, D. E. 1972. Interim Report AMMRC CTR 72-3 (see Ref. 20).

25. McLean, A. F., Fisher, E. A., Bratton, R. J. 1973. Interim Report AMMRC CTR 73-9 (see Ref. 20).

26. Berry, J. P. 1964. Fracture Processes in Polymeric Solids, ed. B. Rosen, 157-194, New York: Wiley.

27. Lange, F. F. 1973. Proc. Fracture Mechanics of Ceramics, ed. R. C. Bradt, D. P. H. Hasselman, F. F. Lange, New York: Plenum, in press.

28. Evans, A. G. 1973 (see Ref. 27).

29. Hahn, G. T., Kanninen, M. F., Rosenfield, A. R. 1972. Ann. Rev. Mat. Sci. 2: 381-404.

30. Wiederhorn, S. M. 1973 (see Ref. 27).

31. Charles, R. J. 1958. J. Appl. Phys. 29:1657-62.

32. Evans, A. G. 1972. J. Mater. Sci. 7:1137-1146.

33. Davidge. R. W., McLaren, J. R., Tappin. G. J. Mater. Sci., in press.

34. Wiederhorn, S. M. 1967. J. Am. Ceram. Soc. 50:407-414.

35. Wiederhorn, S. M. 1966. Materials Science Research 3, ed. W. W. Kriegel, H. Palmore III, 503-528 New York: Plenum.

36. DeSalvo, G. J. 1970. Theory and Structural Design Applications of Weibull Statistics, Rep. WANL-TME-2688, Westinghouse Electric Corp., Astronuclear Laboratory.

37. Weibull, W. 1951. J. Appl. Mech. 18:293-297.

38. Coe, R. F., Lumby, R. J., Pawson, M. F. see Ref. 12, 361-376.

39. Gregory, L. D., Sprvill, C. E. 1964. IAS Conf., Washington, D. C., 33-45.

40. Deeley, G. G., Herbert, J. M., Moore, N. C. 1961. Powder Met. 8:145-151.

41. Oyama, Y., Kamigaito, O. 1971. Japan J. Appl. Phys. 10:1637.

42. Gazza, G. E. 1973. Bul. Am. Ceram. Soc. (abstr.) 52:642.

43. Deeley, G. G. 1972. Brit. Pat. 1,273,145.

44. Wild, S., Grieveson, P., Jack, K. H., see Ref. 12, 385-395.

45. Priest, H. F., Burns, F. C., Priest, G. L., Skaar, E. C. 1973. J. Am. Ceram. Soc. 56:395.

46. Oyama, Y., Kamigaito, O. 1973. Yogyo-Kyokai-Shi, 81:290-293.

47. Jack, K. H., Wilson, W. I. 1972. Nat. Phys. Sci., 238:28-29.

48. Oyama, Y. 1972. Japan J. Appl. Phys. 11:1572.

49. Coe, R. F. 1967. Brit. Pat. 1,092,637.

50. Lange, F. F. J. Am. Ceram. Soc., in press.

51. Rhodes, W. H., Cannon, R. M., Jr. 1972. High Temperature Compounds for Turbine Vanes, Rept. NASA-CR 120966.

52. Lange, F. F., Terwilliger, G. R. 1972. Fabrication and Properties of Silicon Compounds, Tech. Rep. AD-738865,

53. Colquhoun, I., Thompson, D. P., Wilson, W. I., Grieveson, P., Jack, K. H. 1973. Proc. Brit. Ceram. Soc. 22:181-195.

54. Wild, S., Grieveson, P., Jack, K. H., Latimer, M. J., see Ref. 12, 377-384.

55. Terwilliger, G. R., Lange, F. F., J. Am. Ceram. Soc., in press.

56. Evans, A. G., Sharp, J. V. 1971. J. Mater. Sci. 6:1292-1302.

57. Kossowsky, R. J. Mater. Sci., in press.

58. Ref. 20, 97-98.

59. Lange, F. F. 1973. J. Am. Ceram. Soc. 56:445-450.

60. Ref. 25, 149-153.

61. Terwilliger, G. R., Lange, F. F., unreported observations.

62. White, E. W. Private communication.

63. Lumby, R. J., Coe, R. F. 1970. Proc. Brit. Ceram. Soc. 15:91-101.

64. Baurngartner, H. R., Richerson, D. W., see Ref. 27.

65. Lange, F. F. J. Am. Ceram. Soc., in press.

66. Richerson, D. W. 1973. Bul. Am. Ceram. Soc., 52:560-562.

67. Evans, A. G. and Wiederhorn, S. M. J. Mat. Sci., in press.

68. Iskoe, J. L., Lange, F. F. 1973. Bul. Am. Ceram. Soc. (abstr.) 52:646.

69. Kossowsky, R., Frazier, W. C. 1973. Bul. Am. Ceram. Soc. (abstr.) 52:426, also see Ref. 25 :143.

70. Knippenberg, W. F. 1963. Philips Res. Rep. 18:161-274.

71. Alliegro, R. A., Coffin, L. B., Tinklepaugh, J. R. 1956. J. Am. Ceram. Soc., 39:386-389.

72. Antonova, N. D., Kalinina, A. A., Kudryavtsev, V. I. 1962. Sov. Powder Met. & Met. Ceram., 444-449.

73. Prochazka, S. 1972. Investigation of Ceramics for High-Temperature Turbine Vanes, Final Rep. Contract No. N00019-72-C-0129.

74. Lange, F. F. 1973. Task I: Hot-Pressing Behavior of SiC Powders With Additions of Al_2O_3, see Ref. 15.

75. Prochazka, S., Charles, R. J. 1973. Strength of Boron-Doped, Hot-Pressed SiC, General Electric Rep. 73CRD169.

76. Weaver, G. O., Olson, B. A. 1972. Bul. Am. Ceram. Soc. (abstr.) 51:429.

77. Lange, F. F. 1973. Strength Behavior of Hot-Pressed SiC, Final Rep., ONR Contract N00014-68-C-0323.

78. Kossowsky, R., Miller, D. G., Diaz, E. S. 1973. Bul. Am. Ceram. Soc. (abstr.) 52:646.

79. Prochazka, S., Charles, R. J. 1973. See Ref. 27.

80. Schaller, R. J., Rahaim, P. J. 1973. ASME Pub. 73-GT-46, Transient Analysis of Ceramic Vanes for Heavy Duty Gas Turbines, see Ref. 14.

81. Evans, A. G., Wiederhorn, S. M. 1973. NBS Rep. NBSIR 73-147; also, Intl. J. Frac. Mech., in press.

82. Lange, F. F. 1973. Task III: Relative Resistance of Dense Si_3N_4 and SiC to Surface Damage Introduced by Hertzian Contact Stresses, see Ref. 15.

83. Frank, F. C., Lawn, B. R. 1967. Proc. Roy. Soc. 299A:291-306.

84. Roesler, F. C. 1956. Proc. Phys. Soc. 69B:55-60.

85. Tilly, G. P., Sage, W. 1969. ASME Pub. 69-WA/Met-6.

86. Wheildon, W. M., Baumgartner, H. R., Sundberg, D. V., Torti, M. L. 1973. Ceramic Materials in Rolling Contact Bearings, Final Rep. NAVAIR N00019-72-C-0299.

87. Singhal, S. C. 1972. Corrosion Behavior of Si_3N_4 and SiC in Turbine Atmospheres, Proc. Tri-Service Conf. on Corrosion, Houston, Texas.

88. Kossowsky, R. 1973. J. Am. Ceram. Soc. 56:531-535.

89. Singhal, S. C. in press.

90. Singhal, S. C., Lange, F. F. 1973. Bul. Am. Ceram. Soc. (abstr.) 52:646.

91. Batha, D. H., Whitney, E. D. 1973. J. Am. Ceram. Soc. 56:365-369.

92. Rosner, D. E., Allendorf, H. D. 1970. J. Phys. Chem., 74:1829-1839.

93. Francis, T. L., Coble, R. L. 1965. J. Am. Ceram. Soc., 49:269.

94. Brennan, J. J. 1973. Development of Fiber Reinforced Ceramic Matrix Composites, United Aircraft Res. Lab. Rep. M911647-1.

FOOTNOTES

1. The commercial materials discussed are those manufactured by the Norton Co., Worcester, Massachusetts.

2. See Ref. 7 for a general review of this subject pertaining to ceramics.

3. See Refs. 26-28 for a general review of this subject.

4. See Ref. 36 for a general review of Weibull statistics.

5. A similar concept can be applied to surface areas instead of volume elements.

6. Weibull also suggested a three parameter function.

7. Calculations which assume that 5 volume % of the liquid phase is evenly spread along the boundaries of a 1 μm average grain size material result in a boundary phase thickness of < 200 Å which would be difficult to detect.

8. The streaks, which can be considered as crack precursors, can be eliminated by either allowing sufficient grain growth to occur during densification or by minimizing the presence of the laminar void space caused by density gradients during the cold pressing of the powder compacts.

FIGURE CAPTIONS

FIG. 1 -- Room temperature fracture surface topography of Si_3N_4 illustrating BN inclusion at fracture origin

FIG. 2 -- Flexural strength of Norton HS-110 and HS-130 Si_3N_4 (weak direction) vs temperature (air ambient). (65).

FIG. 3 -- Flexural strength vs stressing rate data for Norton HS-130 Si_3N_4 (weak direction, air ambient) at various temperatures (65).

FIG. 4 -- Crack velocity (v) vs stress intensity factor (K) data for Norton HS-130 Si_3N_4 at various temperatures (67).

FIG. 5 -- Fracture surface topograph of Si_3N_4 at high temperatures illustrating rough, crack shaped area caused by plastic deformation during sub-critical crack growth. Arrow points to BN inclusion.

FIG. 6 -- Flexural strength vs impurity content for Si_3N_4 fabricated with pure β-Si_3N_4 (+ 5 wt % MgO) powders. Impurities added prior to hot-pressing (68).

FIG. 7 -- Steady-state creep data for Norton HS-110 and HS-130 Si_3N_4 (69).

FIG. 8 -- Polished and etched section of SiC hot-pressed with 0.10 volume fraction of Al_2O_3 (74).

FIG. 9 -- Flexural strength of SiC vs the amount of Al_2O_3 used for fabrication.

FIG. 10 -- Flexural strength vs stressing rate for Norton SiC containing < 100 ppm Ca and for experimental Sic(+ 2 volume fraction Al_2O_3) containing 0.2 wt % CaO which was intentionally added prior to hot-pressing.

FIG. 11 -- Flexural strength of Si_3N_4 (weak direction) and SiC vs a spherical indenter was forced onto their surface.

FIG. 12 -- Oxidation behavior of Norton HS-130 Si_3N_4 and SiC (87).

ACKNOWLEDGMENTS

The author is grateful to the Office of Naval Research and the Naval Air Systems Command for support of the author's work in this field and in the preparation of this review. The various authors who supplied reprints, manuscripts and reports are acknowledged with thanks.

TABLE I. EFFECT OF SPECIMEN PREPARATION ON FLEXURAL STRENGTH OF HOT-PRESSED SiC

Specimen Preparation	Flexural Strength (MN/m^2)	Standard Deviation (%)
Diamond Cut	503	± 22
3 Sides Ground	630	± 15
3 Sides Ground Edges Beveled	670	± 9

TABLE II. MECHANICAL PROPERTIES OF Si_3N_4 HOT-PRESSED FROM α- AND β-PHASE POWDERS

Major Phase		Flexural Strength	K_c	E	γ
Powder	After Hot-Pressing	(MN/m^2)	($MN/m^{-3/2}$)	(GN/m^2)	(N/M)
α-Si_3N_4	β-Si_3N_4	656	6.53	307	69.5
β-Si_3N_4	β-Si_3N_4	375	3.11	307	15.8

Fig. 1

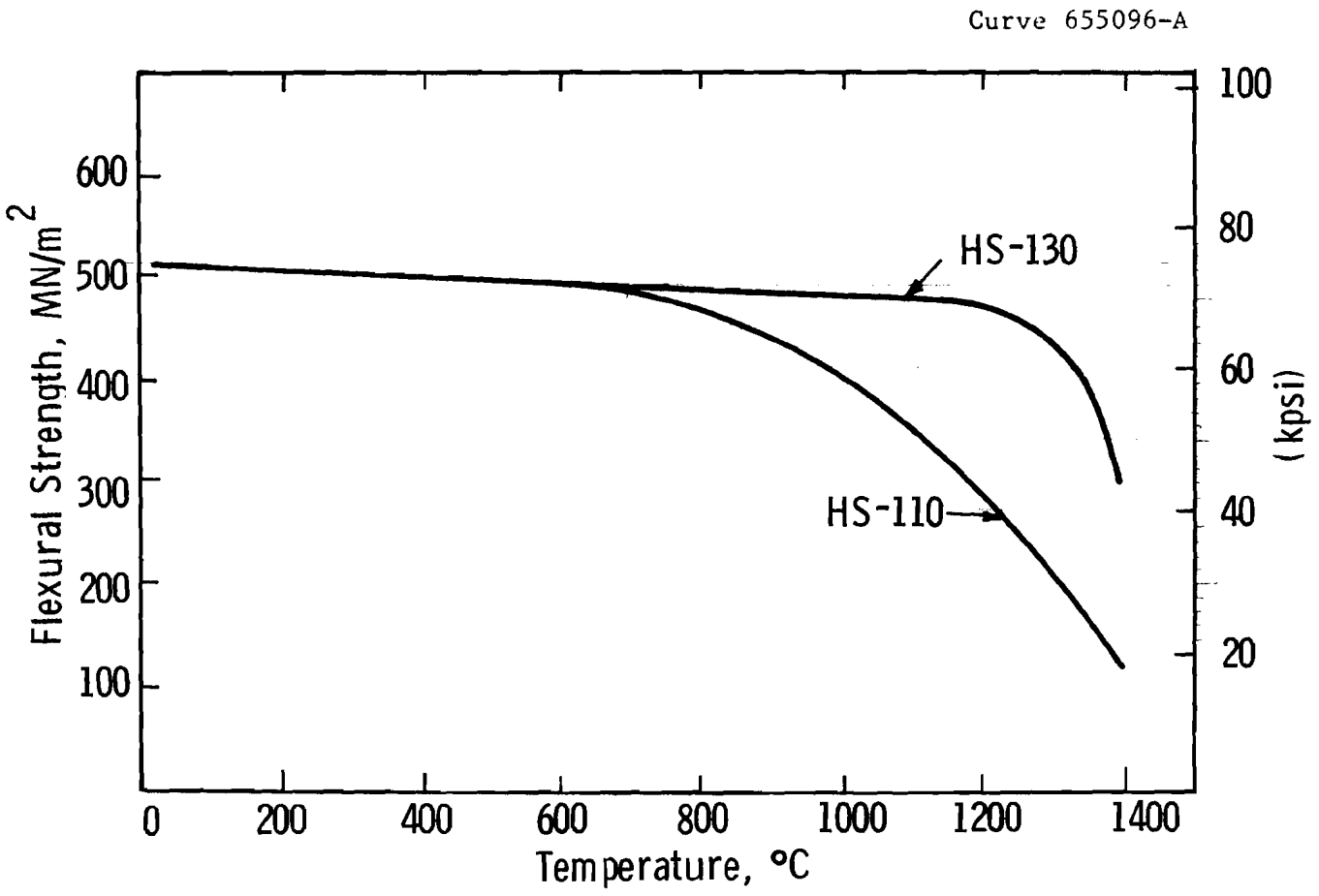
Curve 655096-A
Flexural Strength, MN/m^2
600
500
400
300
200
100
100
80
60
40
20
(kpsi)
HS-130
HS-110
0
200
400
600
800
1000
1200
1400
Temperature, °C

Fig. 2

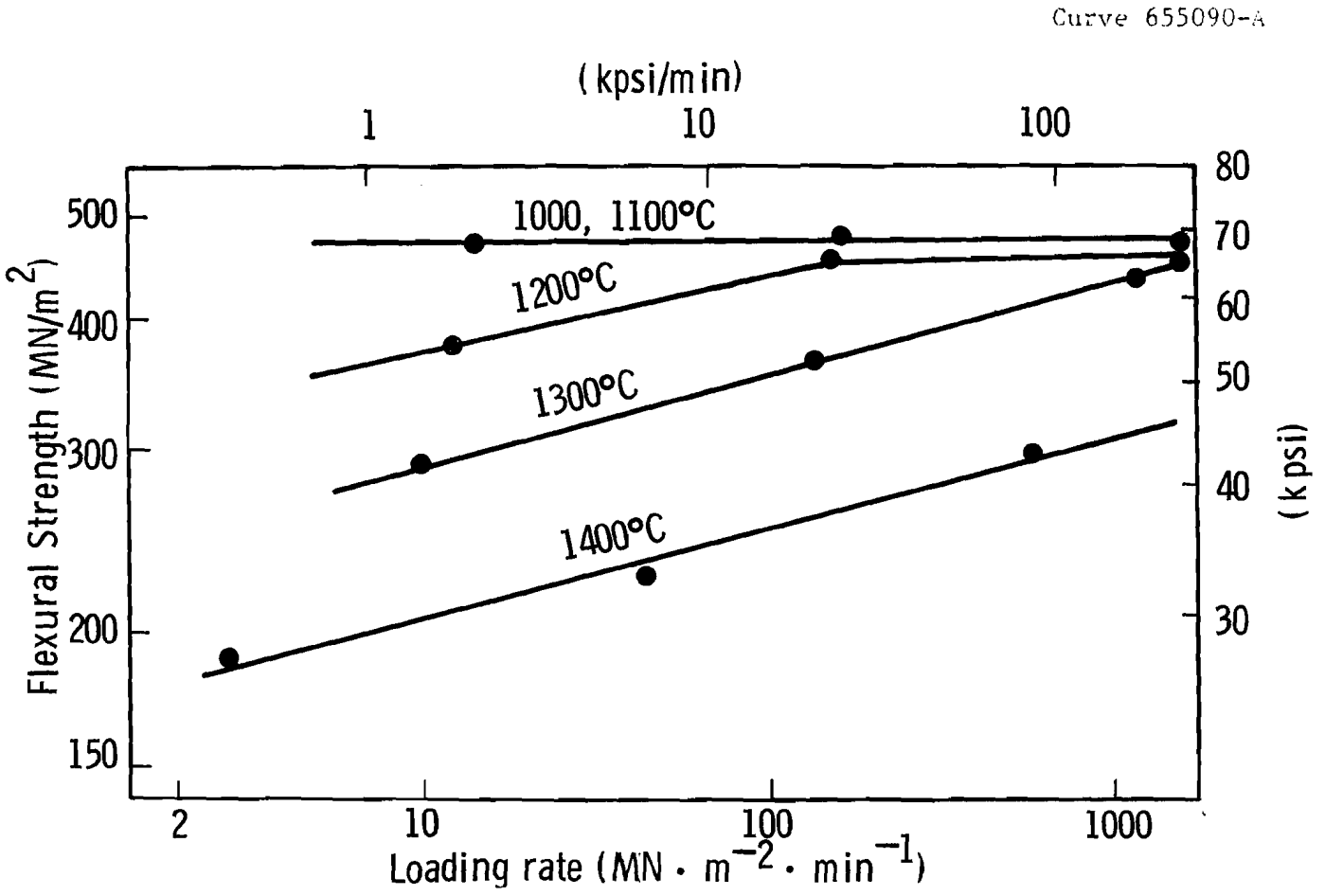
Curve 655090-A
(kpsi/min)
1
10
100
500
400
300
200
150
80
70
60
50
40
30
(kpsi)
1000, 1100°C
1200°C
1300°C
1400°C
Flexural Strength (MN/m^2)
2
10
100
1000
Loading rate (MN · m^{-2} · min^{-1})

Fig. 3

Curve 655091-A

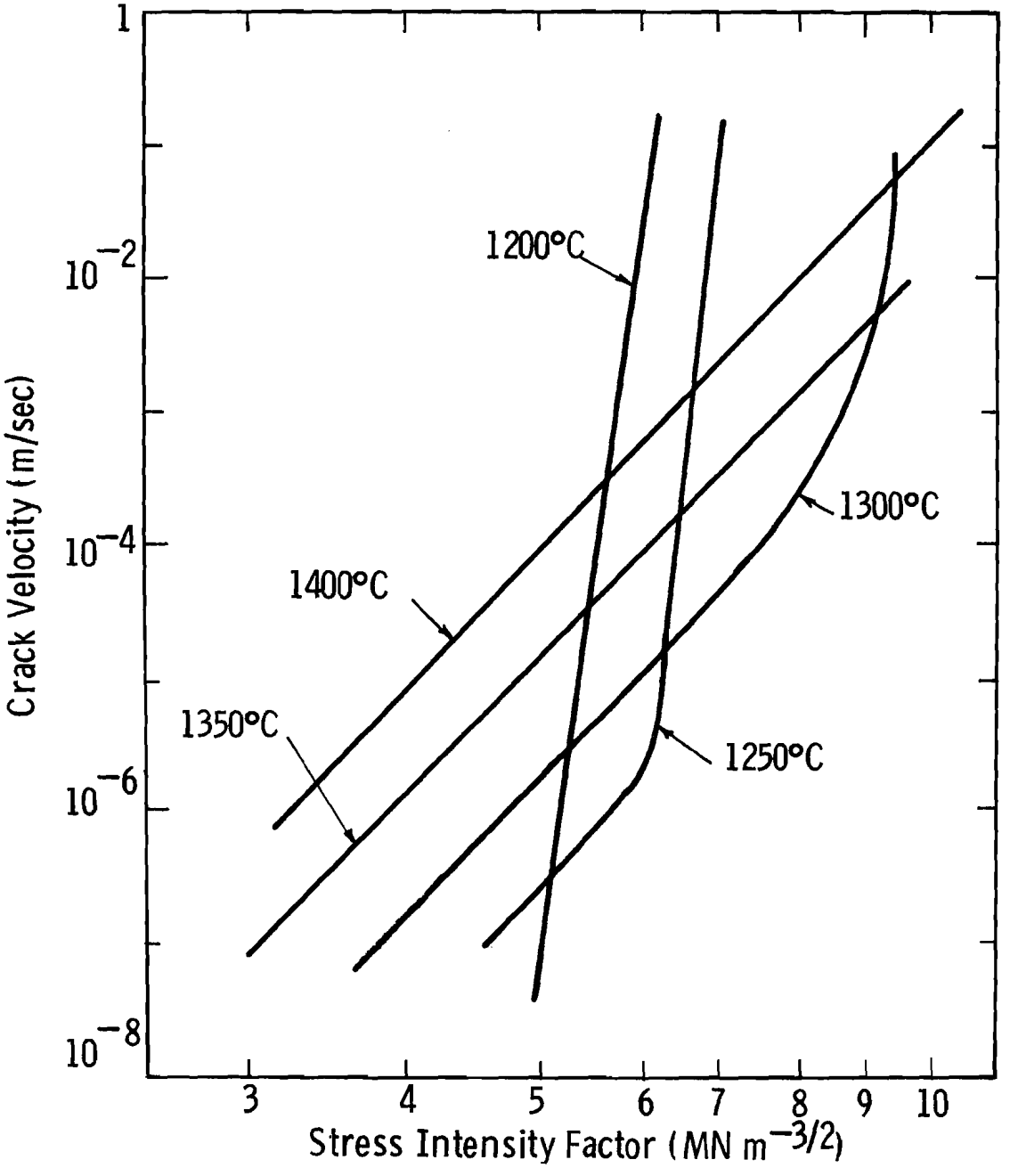

Fig. 4

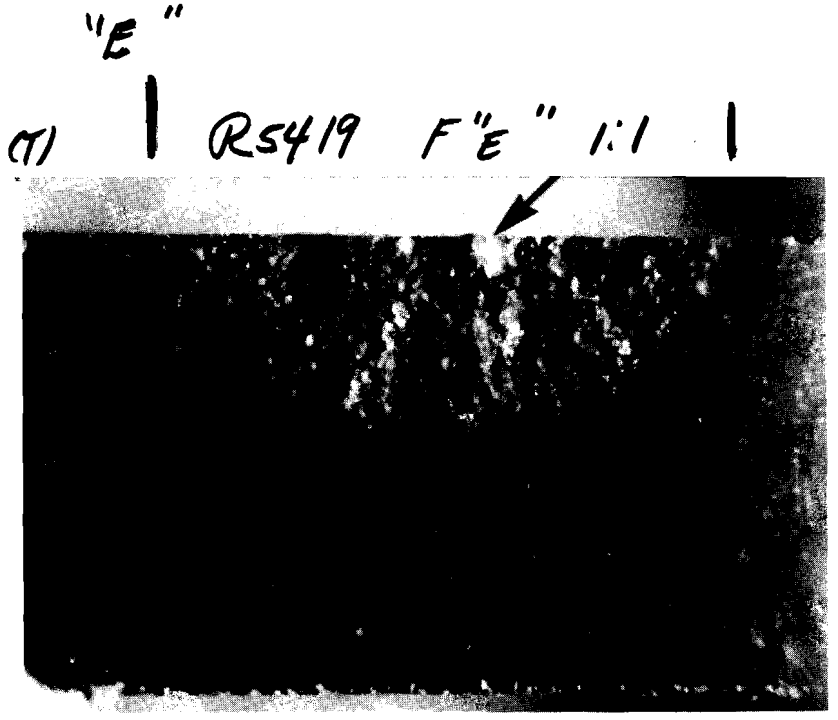

Fig. 5

Curve 655093-A

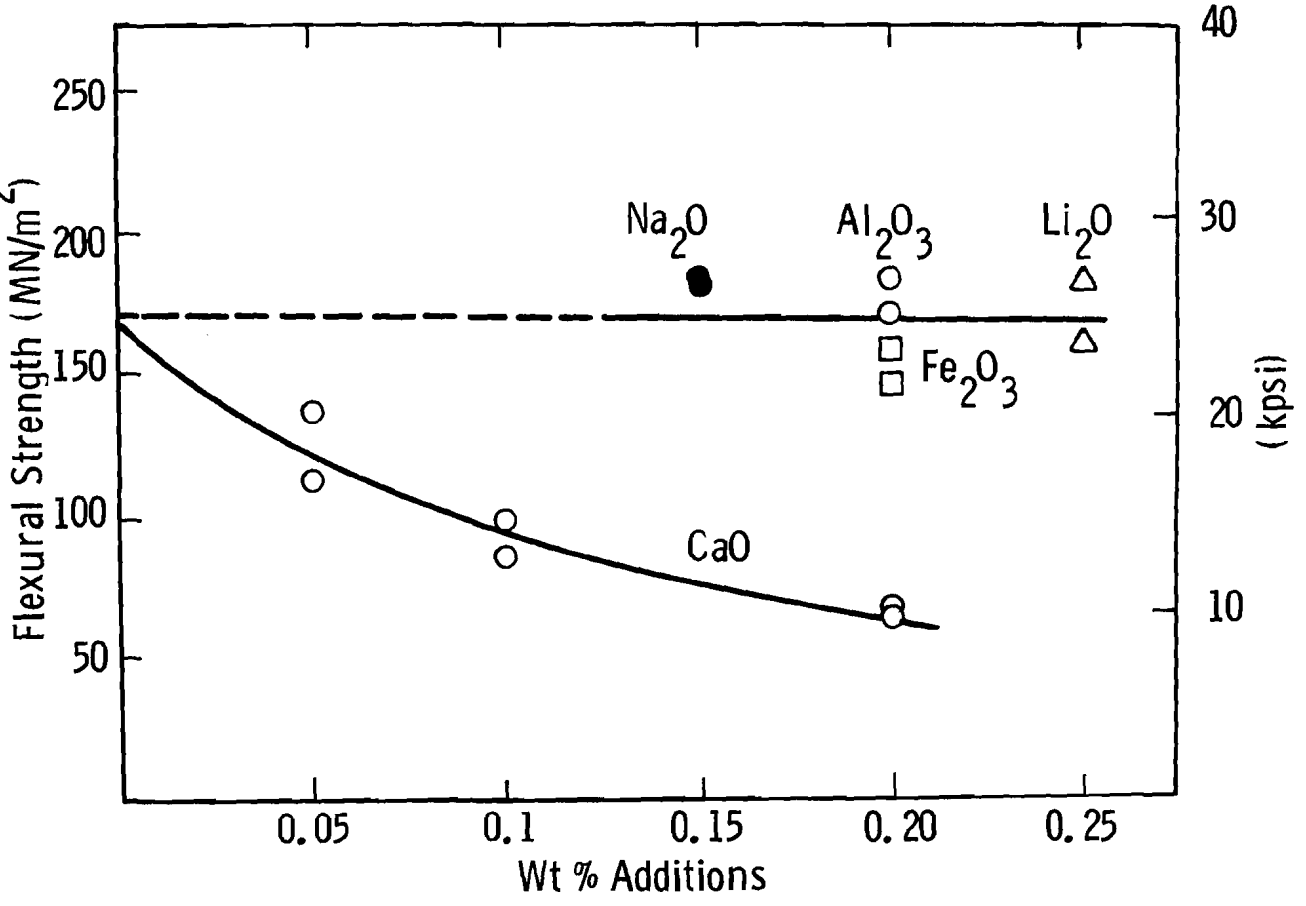

Fig. 6

Curve 655095-A

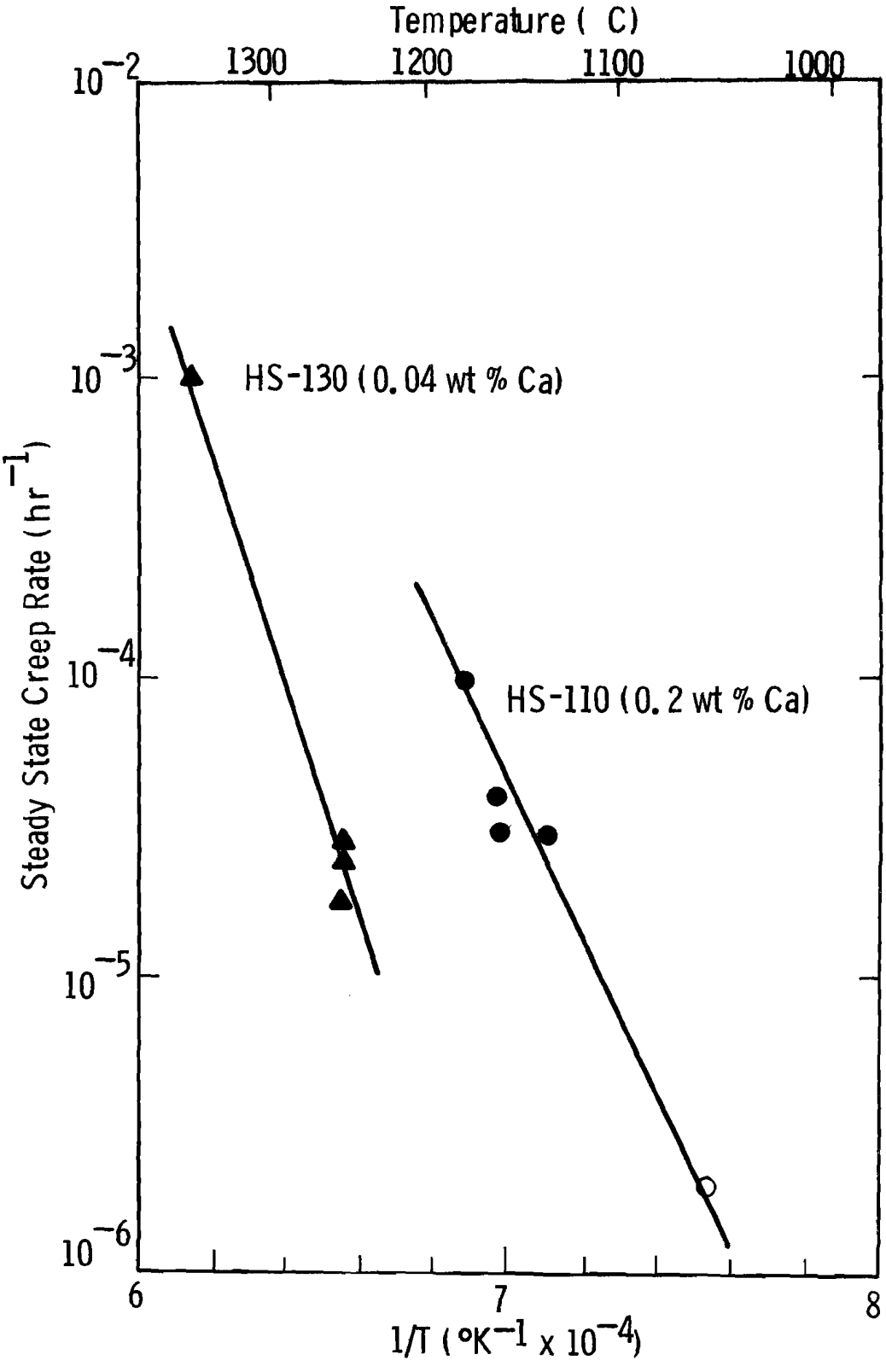

Fig. 7

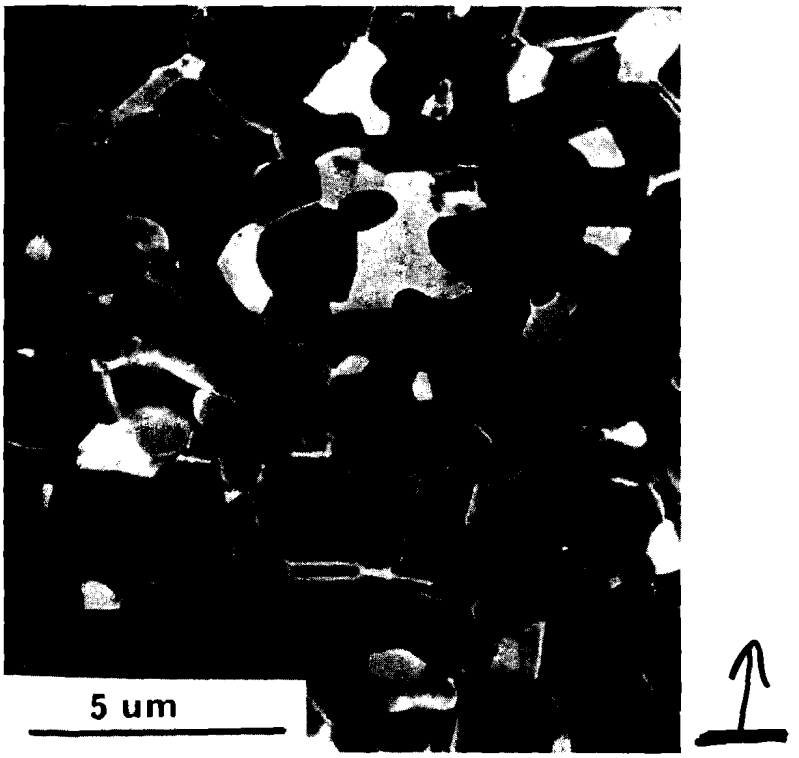

Fig. 8

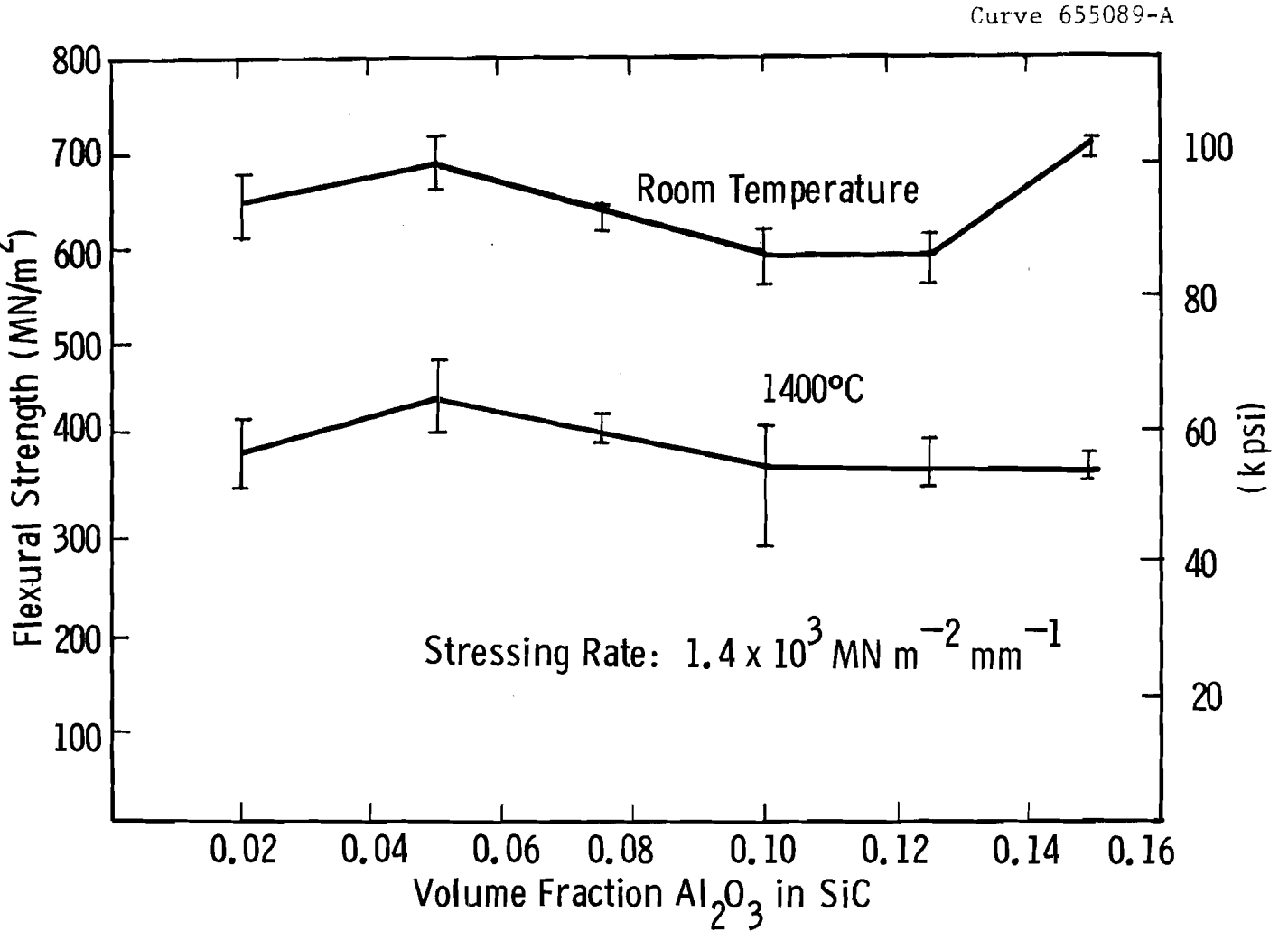
Curve 655089-A
800
700
600
500
400
300
200
100
Flexural Strength (MN/m^2)
100
80
60
40
20
(k psi)
Room Temperature
1400°C
Stressing Rate: 1.4 x 10^3 MN m^{-2} mm^{-1}
0.02
0.04
0.06
0.08
0.10
0.12
0.14
0.16
Volume Fraction Al_2O_3 in SiC

Fig. 9

Curve 655094-A

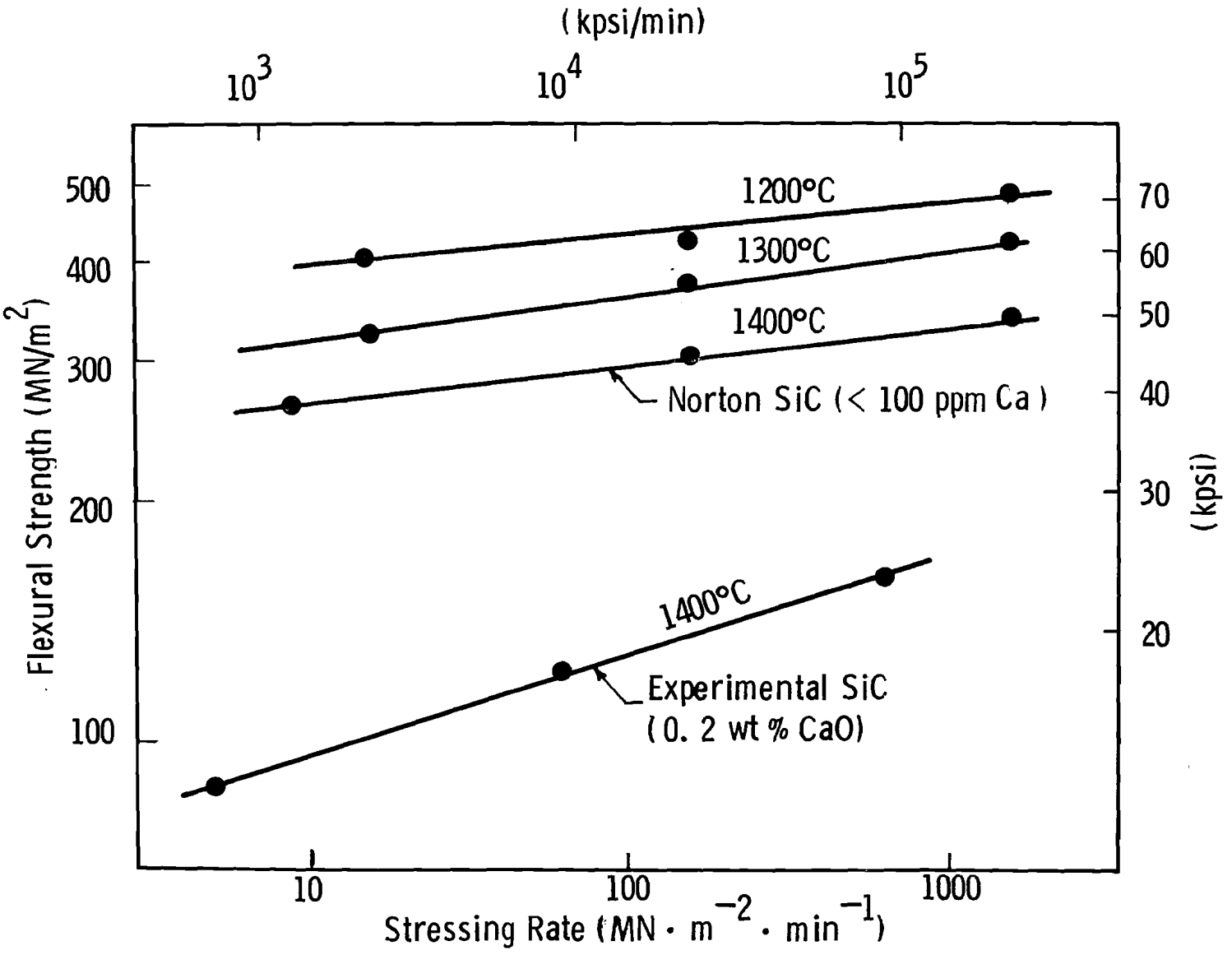

Fig. 10

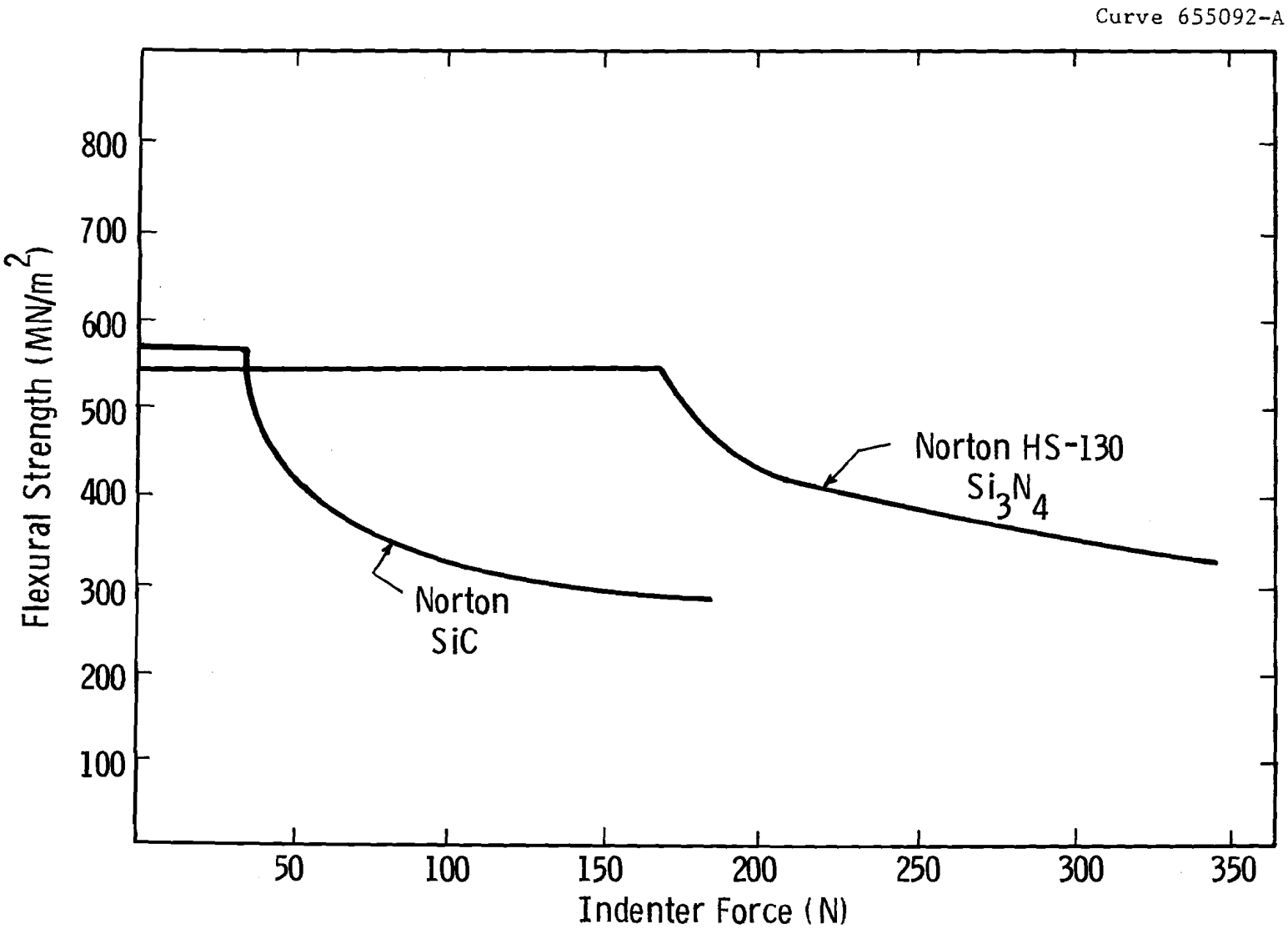
Curve 655092-A
Flexural Strength (MN/m^2)
800
700
600
500
400
300
200
100
50
100
150
200
250
300
350
Indenter Force (N)
Norton HS-130
Si_3N_4
Norton
SiC

Fig. 11

Curve 655088-A

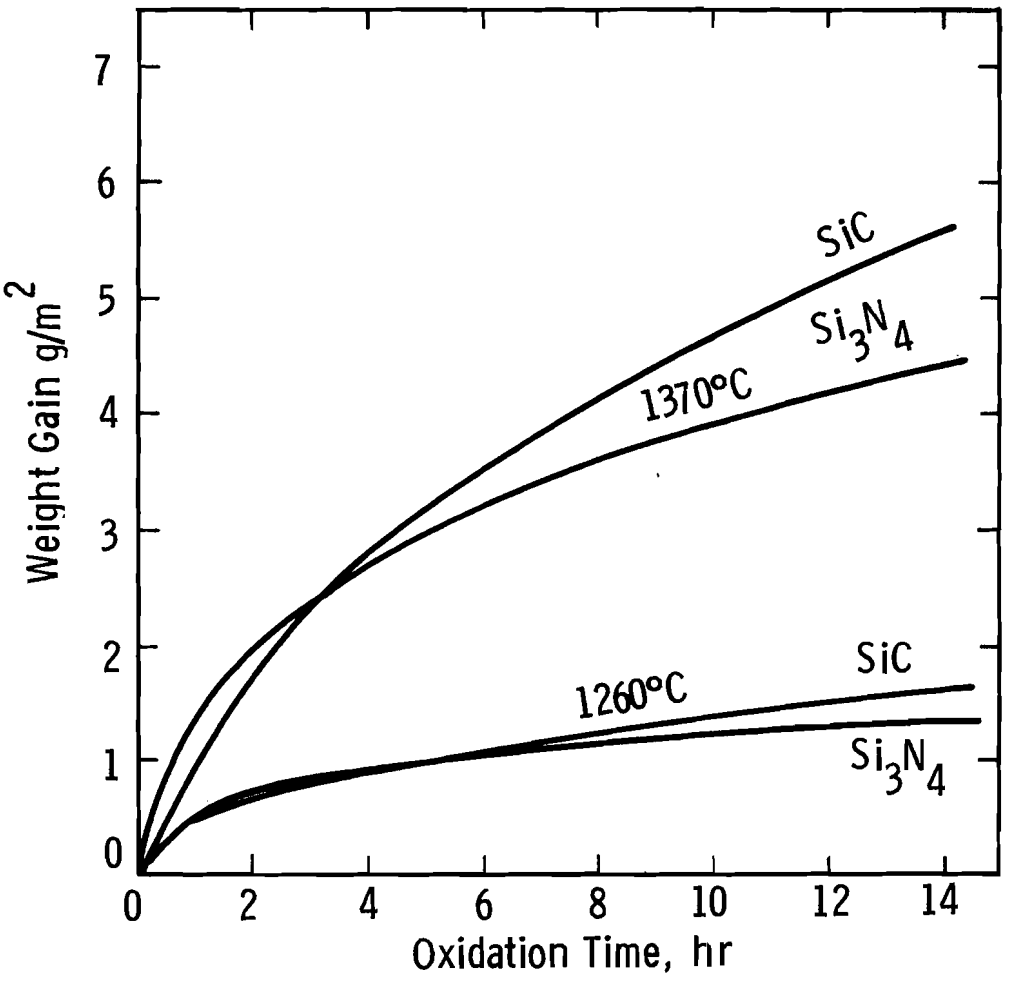

Fig. 12

DISTRIBUTION LIST

Office of Naval Research
Department of the Navy
Arlington, VA 22217

Attn: Code 471

Director
Office of Naval Research
Branch Office
495 Summer Street
Boston, MA 02210

Commanding Officer
Office of Naval Research
New York Area Office
207 West 24th Street
New York, NY 10011

Director
Office of Naval Research
Branch Office
219 South Dearborn Street
Chicago, IL 60604

Director
Office of Naval Research
Branch Office
1030 East Green Street
Pasadena, CA 91101

Commanding Officer
Office of Naval Research
San Francisco Area Office
50 Fell Street
San Francisco, CA 94102

Commanding Officer
Naval Weapons Laboratory
Dahlgren, VA 22448

Attn: Research Division

Director
Naval Research Laboratory
Washington, DC 20390

Attn: Technical Information
Officer, Code 2000
Code 2020
Code 6000
Code 6100
Code 6300
Code 6400
Code 2029 (ONRL)

Commander
Naval Air Systems Command
Department of the Navy
Washington, DC 20360

Attn: Code AIR 320A
Code AIR 5203

Commander
Naval Ordnance Systems Command
Department of the Navy
Washington, DC 20360

Attn: Code ORD 033

Commanding Officer
Naval Air Development Center
Aeronautical Materials Div.
Johnsville
Warminster, PA 18974

Attn: Code MAM

Commanding Officer
Naval Ordnance Laboratory
White Oak, Silver Spring, MD 20910

Attn: Code 210

DISTRIBUTION LIST (cont'd)

Commander
Naval Ship Systems Command
Department of the Navy
Washington, DC 20360

Attn: Code 0342

Commanding Officer
Naval Civil Engineering Laboratory
Port Hueneme, CA 93041

Attn: Code L70

Commander
Naval Ship Engineering Center
Department of the Navy
Washington, DC 20360

Attn: Code 6101

Naval Ships R&D Laboratory
Annapolis Division
Annapolis, MD 21402

Attn: Code A800

Commanding Officer
Naval Ships R&D Center
Washington, DC 20007

Attn: Code 747

U.S. Naval Postgraduate School
Monterey, CA 93940

Attn: Dept. of Chemistry and
Material Science

Commander
Naval Weapons Center
China Lake, CA 93555

Attn: Code 5560

Commander
Naval Undersea Warfare Center
Pasadena, CA 92152

Scientific Advisor
Commandant of the Marine Corps
Washington, DC 20380

Attn: Code AX

Commanding Officer
Army Research Office, Durham
Box CM, Duke Station
Durham, NC 27706

Attn: Metallurgy & Ceramics Div.

Office of Scientific Research
Department of the Air Force
Washington, DC 20333

Attn: Solid State Div. (SRPS)

Defense Documentation Center
Cameron Station
Alexandria, VA 22314

National Bureau of Standards
Washington, DC 20234

Attn: Metallurgy Division
Inorganic Materials Div.

Atomic Energy Commission
Washington, DC 20545

Attn: Metals & Materials Branch

Argonne National Laboratory
Metallurgy Division
P. O. Box 299
Lemont, IL 60439

DISTRIBUTION LIST (cont'd)

Brookhaven National Laboratory
Technical Information Division
Upton, Long Island, NY 11973

Attn: Research Library

Director
Metals and Ceramics Division
Oak Ridge National Laboratory
P. O. Box X
Oak Ridge, TN 37830

Los Alamos Scientific Laboratory
P. O. Box 1663
Los Alamos, NM 87544

Attn: Report Librarian

Commanding Officer
Army Materials and Mechanics
Research Center
Watertown, MA 02172

Attn: Res. Programs Office (AMXMR-P)

Library
Bldg. 50, Room 134
Lawrence Radiation Laboratory
Berkeley, CA 94720

Commanding Officer
Naval Underwater Systems Center
Newport, RI 02844

Aerospace Research Laboratories
Wright-Patterson AFB
Building 450
Dayton, OH 45433

Defense Metals Information Center
Battelle Memorial Institute
505 King Avenue
Columbus, OH 43201

Army Electronics Command
Evans Signal Laboratory
Solid State Devices Branch
c/o Senior Navy Liaison Officer
Fort Monmouth, NJ 07703

Commanding General
Department of the Army
Frankford Arsenal
Philadelphia, PA 19137

Attn: ORDBA-1320, 64-4

Executive Director
Materials Advisory Board
National Academy of Sciences
2101 Constitution Avenue, N.W.
Washington, DC 20418

NASA Headquarters
Washington, DC 20546

Attn: Code RRM

Air Force Materials Lab
Wright-Patterson AFB
Dayton, OH 45433

Attn: MAMC
MAAM

Deep Submergence Systems Project
Washington, DC 20360

Attn: DSSP-00111

DISTRIBUTION LIST (cont'd)

Advanced Research Projects Agency
Washington, DC 20301

Attn: Director, Materials Sciences

Army Research Office
3045 Columbia Pike
Arlington, VA 22204

Attn: Dr. T. E. Sullivan

Department of Interior
Bureau of Mines
Washington, DC 20240

Attn: Science & Engineering
Advisor

Defense Ceramics Information Center
Battelle Memorial Institute
505 King Avenue
Columbus, OH 43201

National Aeronautics & Space Adm.
Lewis Research Center
21000 Brookpark Road
Cleveland, OH 44135

Attn: Librarian

Naval Missile Center
Materials Consultant
Code 3312-1
Point Mugu, CA 93041

Commanding Officer
Naval Weapons Center Corona Labs.
Corona, CA 91720

Commander
Naval Air Test Center
Weapons Systems Test Div. (Code 01A)
Patuxent River, MD 20670

Director
Ordnance Research Laboratory
P. O. Box 30
State College, PA 16801

Commander
Naval Undersea Warfare Center
271 Catalina Boulevard
San Diego, CA 92152

Director
Applied Physics Laboratory
Johns Hopkins University
8621 Georgia Avenue
Silver Spring, MD 20901

Director Applied Physics Laboratory
University of Washington
1013 Northeast Fortieth Street
Seattle, WA 98105

Materials Sciences Group, Code S130.1
Navy Electronics Laboratory
271 Catalina Boulevard
San Diego, CA 92152

Professor R. Roy
Materials Research Laboratory
Pennsylvania State University
University, Park, PA 16802

Professor D. H. Whitmore
Department of Metallurgy
Northwestern University
Evanston, IL 60201

Professor J. A. Pask
Department of Mineral Technology
University of California
Berkeley, CA 94720

Professor D. Turnbull
Div. of Engineering & Applied Science
Harvard University
Pierce Hall
Cambridge, MA 02100

DISTRIBUTION LIST (cont'd)

Dr. T. Vasilos
AVCO Corporation
Research & Advanced Development Div.
201 Lowell Street
Wilmington, MA 01887

Dr. H. A. Perry
Naval Ordnance Laboratory
Code 230
Silver Spring, MD 20910

Dr. Paul Smith
Crystals Branch, Code 6430
Naval Research Laboratory
Washington, DC 20390

Dr. A. R. C. Westwood
RIAS Division
Martin-Marietta Corporation
1450 South Rolling Road
Baltimore, MD 21227

Dr. R. H. Doremus
General Electric Corporation
Metallurgy and Ceramics Laboratory
Schenectady, NY 12301

Professor G. R. Miller
Dept. of Ceramic Engineering
University of Utah
Salt Lake City, UT 84112

Dr. Phillip L. Farnsworth
Materials Department
Battelle Northwest
P. O. Box 999
Richland, WA 99352

Mr. G. H. Haertling
Ceramic Division
Sandia Corp.
Albuquerque, NM 87101

Mr. I. Berman
Army Materials & Mechanics
Research Center
Watertown, MA 02171

Professor H. A. McKinstry
Pennsylvania State University
Materials Research Laboratory
University Park, PA 16802

Professor T. A. Litovitz
Physics Department
Catholic University of America
Washington, DC 20017

Dr. R. J. Stokes
Honeywell, Inc.
Corporate Research Center
500 Washington Ave., South
Hopkins, MN 55343

Dr. Harold Liebowitz
Dean of Engineering
George Washington University
Washington, DC 20006

Dr. H. Kirchner
Ceramic Finishing Company
P. O. Box 498
State College, PA 16801

Professor A. H. Heuer
Case Western Reserve University
University Circle
Cleveland, OH 44106

Dr. D. E. Niesz
Battelle Memorial Institute
505 King Avenue
Columbus, OH 43201

Dr. F. A. Kroger
University of Southern California
University Park
Los Angeles, CA 90007

Dr. S. M. Wiederhorn
Inorganic Materials Division
National Bureau of Standards
Washington, DC 20234

DISTRIBUTION LIST (cont'd)

Dr. Co. Hulse
United Aircraft Research Labs
United Aircraft Corporation
East Hartford, CT 06108

Dr. R. M. Haag
Space Systems Division
AVCO Corporation
Lowell Industrial Park
Lowell, MA 01851

Stanford University
Dept. of Materials Sciences
Stanford, CA 94305

Dr. R. K. MacCrone
Dept. of Materials Engineering
Rensselaer Polytechnic Institute
Troy, NY 12181

Dr. D. C. Mattis
Belfer Graduate School of Science
Yeshiva University
New York, NY 10033

Professor R. B. Williamson
College of Engineering
University of California
Berkeley, CA 94720

Professor R. W. Gould
Department of Metallurgical
and Materials Engineering
College of Engineering
University of Florida
Gainesville, FL 32601

Professor V. S. Stubican
Department of Materials Science
Ceramic Science Section
Pennsylvania State University
University Park, PA 16802

Dr. R. C. Anderson
General Electric R&D Center
P. O. Box 8
Schenectady, NY 12301

Mr. W. A. Sanders
NASA
Lewis Research Center
Cleveland, OH 44135

Library
Stellite Division
Cabot Corporation
1020 W. Park Avenue
Kokomo, IN 46901

Dr. W. Haller
Chief, Inorganic Glass Section
National Bureau of Standard
Washington, D.C. 20234

Professor M. H. Manghnani
University of Hawaii
Hawaii Institute of Geophysics
2525 Correa Road
Honolulu, HI 96822

UNCLASSIFIED

Security Classification

DOCUMENT CONTROL DATA - R&D

(Security classification of title, body of abstract and indexing annotation must be entered when the overall report is classified)

1. ORIGINATING ACTIVITY (Corporate author)	2a. REPORT SECURITY CLASSIFICATION
Westinghouse Research & Development Center	UNCLASSIFIED
	2b GROUP

3. REPORT TITLE

STRONG, HIGH-TEMPERATURE CERAMICS

4. DESCRIPTIVE NOTES (Type of report and inclusive dates)

Interim Technical Report

5. AUTHOR(S) (Last name, first name, initial)

F. F. Lange

6. REPORT DATE	7a. TOTAL NO. OF PAGES	7b. NO. OF REFS
February 6, 1974	76	94

8a. CONTRACT OR GRANT NO.	9a. ORIGINATOR'S REPORT NUMBER(S)
N00014-68-C-0323	
b. PROJECT NO.	73-9D4-KERAM-P1
c.	9b. OTHER REPORT NO(S) (Any other numbers that may be assigned this report)
d.	None

10. AVAILABILITY/LIMITATION NOTICES

Reproduction in whole or in part is permitted for any purpose of the U. S. Government. Distribution of this document is UNLIMITED.

11. SUPPLEMENTARY NOTES	12. SPONSORING MILITARY ACTIVITY
	Office of Naval Research

13. ABSTRACT

Strong, high-temperature ceramics are defined as those materials that can withstand thermal cycling without failure which is necessary for their use in high temperature structural applications. For this reason, hot-pressed Si_3N_4 and SiC are emphasized. The relations between fabrication parameters, microstructure and strength are presented for both materials. Other structural considerations, viz., resistance to thermal shock, impact and oxidation are reviewed. Finally, current directions for obtaining improved and new materials are discussed.

DD FORM 1 JAN 64 1473

UNCLASSIFIED

Security Classification

14. KEY WORDS	LINK A		LINK B		LINK C	
	ROLE	WT	ROLE	WT	ROLE	WT
ceramics						
silicon nitride						
silicon carbide						
SiAlON						
fabrication						
pressing						
thermal						
oxidation						
impact						
strength						
creep						
size						
shock						
growth						
cracks						

INSTRUCTIONS

1. ORIGINATING ACTIVITY: Enter the name and address of the contractor, subcontractor, grantee, Department of Defense activity or other organization *(corporate author)* issuing the report.

2*a*. REPORT SECURITY CLASSIFICATION: Enter the overall security classification of the report. Indicate whether "Restricted Data" is included. Marking is to be in accordance with appropriate security regulations.

2*b*. GROUP: Automatic downgrading is specified in DoD Directive 5200.10 and Armed Forces Industrial Manual. Enter the group number. Also, when applicable, show that optional markings have been used for Group 3 and Group 4 as authorized.

3. REPORT TITLE: Enter the complete report title in all capital letters. Titles in all cases should be unclassified. If a meaningful title cannot be selected without classification, show title classification in all capitals in parenthesis immediately following the title.

4. DESCRIPTIVE NOTES: If appropriate, enter the type of report, e.g., interim, progress, summary, annual, or final. Give the inclusive dates when a specific reporting period is covered.

5. AUTHOR(S): Enter the name(s) of author(s) as shown on or in the report. Enter last name, first name, middle initial. If military, show rank and branch of service. The name of the principal author is an absolute minimum requirement.

6. REPORT DATE: Enter the date of the report as day, month, year; or month, year. If more than one date appears on the report, use date of publication.

7*a*. TOTAL NUMBER OF PAGES: The total page count should follow normal pagination procedures, i.e., enter the number of pages containing information.

7*b*. NUMBER OF REFERENCES: Enter the total number of references cited in the report.

8*a*. CONTRACT OR GRANT NUMBER: If appropriate, enter the applicable number of the contract or grant under which the report was written.

8*b*, 8*c*, & 8*d*. PROJECT NUMBER: Enter the appropriate military department identification, such as project number, subproject number, system numbers, task number, etc.

9*a*. ORIGINATOR'S REPORT NUMBER(S): Enter the official report number by which the document will be identified and controlled by the originating activity. This number must be unique to this report.

9*b*. OTHER REPORT NUMBER(S): If the report has been assigned any other report numbers *(either by the originator or by the sponsor)*, also enter this number(s).

10. AVAILABILITY/LIMITATION NOTICES: Enter any limitations on further dissemination of the report, other than those imposed by security classification, using standard statements such as:

(1) "Qualified requesters may obtain copies of this report from DDC."

(2) "Foreign announcement and dissemination of this report by DDC is not authorized."

(3) "U. S. Government agencies may obtain copies of this report directly from DDC. Other qualified DDC users shall request through _____."

(4) "U. S. military agencies may obtain copies of this report directly from DDC. Other qualified users shall request through _____."

(5) "All distribution of this report is controlled. Qualified DDC users shall request through _____."

If the report has been furnished to the Office of Technical Services, Department of Commerce, for sale to the public, indicate this fact and enter the price, if known.

11. SUPPLEMENTARY NOTES: Use for additional explanatory notes.

12. SPONSORING MILITARY ACTIVITY: Enter the name of the departmental project office or laboratory sponsoring *(paying for)* the research and development. Include address.

13. ABSTRACT: Enter an abstract giving a brief and factual summary of the document indicative of the report, even though it may also appear elsewhere in the body of the technical report. If additional space is required, a continuation sheet shall be attached.

It is highly desirable that the abstract of classified reports be unclassified. Each paragraph of the abstract shall end with an indication of the military security classification of the information in the paragraph, represented as *(TS)*, *(S)*, *(C)*, or *(U)*.

There is no limitation on the length of the abstract. However, the suggested length is from 150 to 225 words.

14. KEY WORDS: Key words are technically meaningful terms or short phrases that characterize a report and may be used as index entries for cataloging the report. Key words must be selected so that no security classification is required. Identifiers, such as equipment model designation, trade name, military project code name, geographic location, may be used as key words but will be followed by an indication of technical context. The assignment of links, rules, and weights is optional.